High-precision dating of the Kalkarindji large igneous province, Australia and synchronicity with the Early–Middle Cambrian (Stage 4-5) extinction.

F. Jourdan[1*], K. Hodges[1,2], B. Sell[3,4], U. Schaltegger[3], M.T.D. Wingate[5], L.Z. Evins[6], U. Söderlund[7], P.W. Haines[5], D. Phillips[8], T. Blenkinsop[9]

[1]*Western Australian Argon Isotope Facility, Department of Applied Geology and JdL-CMS, Curtin University, Perth, WA 6845, Australia.*

[2]*Sirius Resources, 5 Mumford Place, Balcatta, WA 6021, Australia.*

[3]*Earth Sciences, University of Geneva, Rue des Maraîchers 13, CH-1205 Geneva, Switzerland*

[4]*Earth and Environmental Sciences, University of Michigan, 2534 C C Little, Ann Arbor, MI 48109-1005.*

[5]*Geological Survey of Western Australia, 100 Plain Street, East Perth, WA 6004, Australia*

[6]*Department of Mineralogy, Swedish Museum of Natural History, Box 50007, SE-10504 Stockholm, Sweden, and Swedish Nuclear Fuel and Waste Management Co., Stockholm, Sweden*

[7]*Department of Geology, Lund University, Sölvegatan 12, SE-223 62 Lund, Sweden*

[8]*School of Earth Sciences, The University of Melbourne, Victoria, 3010, Australia*

[9]*School of Earth and Environmental sciences, James Cook University, Townsville, QLD 4811, Australia.*

*Correspondence to: Fred Jourdan, *Western Australian Argon Isotope Facility, Department of Applied Geology and JdL-CMS, Curtin University, Perth, WA 6845, Australia.* f.jourdan@curtin.edu.au. +61424174984

Keywords: large igneous province, geochronology, extinction events, climate change, anoxia

ABSTRACT

The voluminous Kalkarindji flood basalts erupted in Australia during the Cambrian and covered more than 2 million km². New U-Pb and $^{40}Ar/^{39}Ar$ age data from intrusive rocks and lava flows yielded statistically indistinguishable ages at ca. 511 Ma, suggesting a relatively brief emplacement for this province. A zircon age of 510.6 ± 0.5 Ma show that this province is temporally indistinguishable at the hundred thousand year level from the Early–Middle Cambrian (Stage 4-5) boundary age of 510 ± 1 Ma, which marks the first severe extinction of the Phanerozoic and an extended marine anoxia period.

Sulfur concentration measurements ranging from <50 to 1900 µg/g and fractal analysis of extensive explosive volcanic breccias suggest that blasts and phreatomagmatic explosions have contributed to inject large amount of sulfur into the stratosphere. In addition, magma intrusions in oil, gas, and sulfate deposits may have generated significant emission of CH_4 and SO_2 which, along with volcanic gases, would have contributed to destabilize the climate and led to the Cambrian extinction.

INTRODUCTION

Large Igneous Provinces (LIPs) are remnants of significant geodynamic events in Earth history. LIPs are characterized by their vast size (typically millions of square kilometers) and relatively rapid emplacement (~1–3 Ma for the main magma volume; Bryan & Ernst 2008). A thorough temporal control by high-precision geochronological data is essential to understanding the origin, timing, and environmental consequences of LIP eruptions. With advances in radioisotopic dating of both LIPs and mass extinction events, a causal link between the two has been proposed (e.g., Courtillot and Renne, 2003). The best illustrations of this link are for four and perhaps five of the mid-Phanerozoic mass extinction events (Wignall, 2005): mid-Capitanian (Emeishan flood basalts; Wignall et al., 2009); end-Permian (Siberian Traps; Mundil et al., 2004); end-Triassic (Central Atlantic magmatic province or CAMP; Marzoli et al., 1999); and Cretaceous–Paleogene (Deccan Traps; Hofmann et al., 2001). More recently, the Frasnian-Famennian extinction has been tentatively linked to the Viluy Traps (Courtillot et al., 2010), but additional work is required before firmly confirming the synchronicity between the two. Proposed causes for the Cretaceous–Paleogene extinction are controversial as the timing of this extinction is temporally related to a major asteroid impact (Chixculub; e.g., Alvarez et al., 1980). However, no other

large impact–mass extinction pair has been firmly identified in the geological record (Jourdan et al., 2012). Altogether, this suggests that voluminous volcanic activity might play a dominant role in biotic turnovers and climate shifts. Such an hypothesis can be tested by going much further back in time by studying the precise timing of the oldest large igneous province of the Phanerozoic, the Cambrian Kalkarindji flood basalts (Glass and Phillips, 2006) and assessing if this province is synchronous with any significant biotic extinction and climate perturbation.

THE KALKARINDJI LARGE IGNEOUS PROVINCE

Recent geochemical and geochronological data for the Antrim Plateau Volcanics and stratigraphically coeval suites in northern and central Australia (Glass & Philips, 2006), and central Western Australia (Evins et al., 2009) have demonstrated the existence of a large mafic igneous event, the Kalkarindji LIP (Fig. 1). The Kalkarindji LIP is comparable in size to other large igneous provinces, and remnants of lava flows, sills, and dykes can be found across an area of $\geq 2.1 \times 10^6$ km² (Evins et al., 2009). Individual flows reach up to 200 m in thickness, but are more commonly between 20 and 60 m thick. Locally, the Antrim plateau lava pile reaches a maximum preserved cumulative thickness of ca. 1500 m (Glass & Philips, 2006; Evins et al., 2009). Stratigraphic constraints, together with very few accurate high-precision (i.e. internal precision better than ±1%) geochronological results, suggest that the emplacement of the Kalkarindji LIP occurred during the Cambrian period (e.g., Evins et al., 2009). Isotopic ages include one SHRIMP U-Pb zircon age of 508 ± 5 Ma (Macdonald et al., 2005) and three $^{40}Ar/^{39}Ar$ plagioclase ages ranging from 509.0 ± 2.6 Ma to 511.9 ± 1.9 Ma (recalculated from Glass & Philips, 2006 and Evins et al., 2009).

THE EARLY–MIDDLE CAMBRIAN EXTINCTION AND MARINE ANOXIA

Although not yet demonstrated as a full-scale mass extinction because only known from limited geographic areas and restricted to specific groups, the Early–Middle Cambrian (Stage 4-5; EMC) extinction is nerveless the first significant biotic turnover identifiable in the fossil record with ca. 45 % of Genera extinct (cf. compilation by Sepkoski, 1996; Keller, 2005 and recent data from Gozalo et al., 2013). The Cambrian period is characterized by extinction events (Zhuravlev and Wood, 1996; Gozalo et al., 2013) that occurred shortly after the first period of rapid diversification of complex life (the ~545 Ma Cambrian explosion). The more important extinction event occurred during the Toyonian, and has been used to delineate the Early–Middle Cambrian (now Series 2–3, Stage 4–5) boundary. Furthermore, the Stage 4-5 transition is associated with a global sea-level rise, negative $\delta^{13}C$ and positive $\delta^{34}S$ excursions recorded in stratigraphic sections worldwide (e.g. Montañez et al., 2000; Hough et al., 2006).

The age of the EMC (Stage 4-5) boundary is relatively well-constrained by ID-TIMS U-Pb zircon dating and make it suitable for direct comparison with the Kalkarindji LIP. A *minimum* age has been obtained on an ash bed located immediately above the EMC boundary in southern Britain yielding an age of 509.10 ± 0.77 Ma (Harvey et al., 2011) and a *maximum* age of 511 ± 1 Ma (Landing et al., 1998) obtained for an ash bed located right below the EMC boundary, in the upper (but not uppermost) Early Cambrian (Series 2, Stage 4). As such, the two ash beds tightly bracket the EMC boundary between ca. 509 and 511 Ma and we calculate a conservative age of 510 ± 1 Ma as the best estimate of the age of the EMC boundary, in accordance with the most recent stratigraphic timescale (~509 Ma, Cohen et al., 2013).

RESULTS

We acquired relatively well-preserved samples from both the Antrim Volcanics and the Table Hill Volcanics at the opposite extremities of the province (Fig. 1). Descriptions and petrography of the four samples used for isotopic analyses, details of analytical methods and results are presented in detail in (SI Materials and Methods).

We analyzed seven zircons from a fresh surface exposure of the coarse-grained Milliwindi dolerite dyke in the northern Kalkarindji province (Fig. 1). These dates were produced using CA-ID-TIMS at the University of Geneva, on single zircons relative to the new EARTHTIME tracer solution (SI Materials and Methods*) (Table S1*). We calculated a weighted mean $^{238}U/^{206}Pb$ age of 510.67 ± 0.62[1] Ma (MSWD = 2.0; P = 0.09). Twenty-eight baddeleyite crystals, from 25 to 200 µm long, were extracted from a basement intrusive rock from Munro well containing mafic enclaves (Fig. 1) (*SI Materials and Methods*). Six aliquots, each comprising between 2 and 11 crystals, were analyzed using TIMS at the Museum of Natural History in Stockholm. Apparent $^{238}U/^{206}Pb$ ages range from 460 to 528 Ma (Table S2). Analyses define a statistically concordant upper intercept age of 511 ± 5 Ma (MSWD = 1.6; P = 0.20), taken to represent the crystallization age of the sample. A plagioclase sample (#002) separated from dolerite sills intersected by a Officer Basin drill hole (07THD-002) was analyzed by the laser step-heating $^{40}Ar/^{39}Ar$ technique at Curtin University (*SI Materials and Methods*). The sample produced a statistically concordant (MSWD = 0.74; P = 0.69) plateau age of 510 ± 4 Ma, with 74% of total ^{39}Ar released (Table S3) indicating the emplacement age of the sill. Finally, we present S and MgO concentrations of fluid inclusions hosted in plagioclase minerals (5 analyses) and on whole-rock samples (372 analyses) from the Table Hill Volcanics (Table S4; (*SI Materials and Methods*)). Fluid inclusions show S concentrations ranging from 0 to 1254 µg/g. The majority of the S whole-rock data range between 15 and 1900 µg/g with an average value of 884 ± 432 µg/g. In both cases, S does not

[1] All uncertainties in the text are quoted at 2σ and include all sources of errors.

show any co-variation with MgO (0.52 – 6.95 wt%). Six additional whole-rock samples show S enrichment up to ~6963 µg/g).

DISCUSSION

Age of the Kalkarindji magmatism

All the 7 available age results range from 508 ± 5 Ma to 511.9 ± 1.9 Ma (Fig. 2). Independently of the technique used, these ages all agree within uncertainty (MSWD = 1.03; P =0.40; Fig. 2) and suggest an age of ~510 Ma for the province. Nevertheless, it is unlikely that these rocks were emplaced at the exact same time at the hundreds of thousand year timescale but their relative timing is beyond the time resolution achieved by the data. Therefore, only a strict maximum duration of ~3 Ma (the standard deviation of the population is 1.7 Ma) can be tentatively estimated from the current data.

Synchronicity with the Early-middle Cambrian boundary

The U-Pb zircon age of 510.7 ± 0.6 Ma provides a very precise *minimum* age for the onset of Kalkarindji magmatic activity. This age has sufficient precision that it can be compared with the age of the EMC (St. 4-5) boundary of 510 ± 1 Ma. Although, the U-Pb measurements were done using different spikes and in different laboratories more than 10 years apart, the comparatively large uncertainties associated with these data show that the dates are very similar within the time resolution of the technique and demonstrate the synchronicity of the Kalkarindji volcanism and the EMC boundary at the sub-million year level (Fig. 2). It is also worth noting that plagioclase

157 $^{40}Ar/^{39}Ar$ and baddeleyite U-Pb ages alone corroborate this interpretation with a weighted mean
158 age of 510.0 ± 1.4 Ma, which is equally indistinguishable from the age of the EMC boundary.
159
160 *Significance of the Synchronicity between Kalkarindji and the EMC boundary*
161 Synchronicity between LIP volcanism and extinctions has been demonstrated for four of the
162 largest mass extinctions (Fig. 3; Courtillot and Renne, 2003) and where preliminary $^{40}Ar/^{39}Ar$
163 age data for fifth LIP-extinction pair (Viluy traps and Frasnian-Famennian boundary, Courtillot
164 et al., 2010) suggests such a link as well. The agreement between ages for the Kalkarindji LIP
165 and the EMC (St. 4-5) boundary far extends the record of consistent synchronicity between
166 volcanism, climate perturbation and severe extinction to the beginning of the Phanerozoic Era.
167 Although the EMC boundary extinction is not (yet?) defined as a true mass extinction, the
168 extinctions of 45% of the Genera at the time (e.g. Sepkosky, 1996; Keller, 2005), and global
169 isotope excursion (Gozalo et al., 2013) makes it a convincing case for testing the effect of
170 massive volcanism on the climate and biosphere.
171 As a result, the coincidence of large-scale continental volcanism and severe extinction
172 events is significantly more frequent than is expected from pure randomness with a negligible
173 $6x10^{-9}$ % probability (SI Materials and Methods) that such correlation is due to chance alone.
174 This estimate strongly supports a causal relationship between the LIPs and severe extinctions
175 during the Phanerozoic. Two notable exceptions are the Karoo and Parrana-Etendeka LIPs.
176 Whereas the lack of effect of the Karoo LIP on the biosphere is likely due to the peculiar low
177 eruption rate of this province (Jourdan et al., 2008), the reason for the absence of correlation
178 between the Parrana-Etendenka flood basalts and any biotic turnover (Fig. 3) is still unknown.
179

Figure Legends

Fig. 1. Schematic map of the remnant of the Kalkarindji large igneous province (modified after Evins et al., 2009). Ages from this study are shown in bold; those from (Glass and Philips, 2006; Evins et al., 2009; Macdonald et al., 2005) are in normal text. Proterozoic basins are indicated. The Blackfella Rockhole Member volcanic breccia of the Kalkarindji LIP is superimposed (orange) on the Antrim volcanic basalts. The dashed line indicates the likely original extent of the LIP.

Fig. 2. Isotopic ages from the Kalkarindji province and the Early–Middle Cambrian boundary (EMC). (a) (Glass and Philips, 2006); (b) (Evins et al., 2009); (c) this study; (d) (Macdonald et al., 2005); (e) minimum age of the EMC boundary (Harvey et al., 2011); (f) maximum age of the EMC boundary (Landing et al., 1998). $^{40}Ar/^{39}Ar$ ages have been calibrated using the ^{40}K decay constants of (Renne et al., 2011). Uncertainties are at 2σ and include all sources of uncertainty and indicated in bracket. ** U-Pb zircon ages derived from tuff layers and bracketing the EMC boundary.

Fig. 3. Ages of LIP magmatism versus the difference in age between the peak of the magmatism and the temporally closest severe extinction. Black boxes reflect the apparent duration of the main peak of magmatism; Grey boxes reflect uncertainty in the duration due to the current lack of data. *Karoo (grey/white box) is not associated with a mass extinction event but with a global anoxic event and localized ocean turnover (Jourdan et al., 2008). **based on preliminary data from (Courtillot et al., 2010).

Possible causes of the marine anoxia and extinction at the EMC boundary

Although rapid climate change is likely to be the ultimate cause of mass extinctions, the exact trigger mechanisms arising from LIP emplacements that are responsible for these climatic shifts are less clear. Favoured mechanisms include rapid emission of gases (dominantly CO_2 and SO_2, but also CH_4 (methane) halogen and NO_x) either initially dissolved in the magma (Sobolev et al., 2011) or degassed from C-rich and/or sulfate-bearing sediments intruded by dykes and sills (e.g. Svensen et al., 2009). The Kalkarindji LIP is unique in its eruption age and geological setting, and careful observations can bring further constraints to the conditions required to cause large extinction events.

With no extant fauna on land during the Early Cambrian, the extinction mechanism(s) involved must have acted on Cambrian oceans. Sulfur content measured in whole-rock samples and plagioclase melt inclusions from the Table Hill Volcanics display a similar range of values, ranging mostly from <50 to a maximum 1900 µg/g a, with an average of ~884 µg/g (SI Materials and Methods; Table S4). Assuming that either 1900 µg/g or 884 µg/g S represents the possible average values of the rocks *before* degassing, maximum and minimum values of 53% and 15% of S degassing can be calculated. For comparison, the S degassing values estimated for the Deccan and Siberia basalts range from 50 to 90% (e.g., Black et al., 2012). Nevertheless, the total volume of S release is less relevant to any attempt to understand extinction and climate shifts mechanisms because of their ultra-transient presence in the atmosphere (Self et al., 2005). More relevant is the expected maximum atmospheric loading following the largest flow eruptions. To this regard, we report the presence of a ca. 15,000 km² and 70m-thick volcanic breccia (the Blackfella Rockhole Member) near the top of the Antrim Plateau Volcanics sequence (Fig. 1). Our fractal analysis (SI Materials and Methods) shows that these breccias are

of explosive (blast/surge or phreatomagmatic) origin, which drastically increases the potential of gas delivery directly to the stratosphere (Self et al., 2005).

In addition, SO_2 and CH_4 gas emissions could have been caused by contact metamorphism with and/or assimilation of country rocks during the magma ascent (Svensen et al., 2009, Black et al., 2012) and further gas release during eruption. This hypothesis is in agreement with the occurrence of (1) two major sequences of a few hundred meters and up to *two kilometers thick* (average ~800m) of early Neoproterozoic sequences of C-rich evaporite layers (including gypsum anhydrite, and dolostone (Lindsay, 1987) and (2) large quantities of untapped Proterozoic oil and gas source rocks and reservoirs distributed within the ~1 million km² central Australian basins (Bradshaw et al., 1994) (Fig. 1). Metamorphic CH_4 (and halocarbons) emissions caused by magma interaction with oil, gas and C-rich evaporite rocks could be a significant factor as well (Table S6; Ganino and Arndt, 2009) and this possibility is supported by the occurrence of asphalt in vesicles within the Kalkarindji basalts (Bradshaw et al., 1994) and a negative $\delta^{13}C$ recorded at the EMC boundary.

Finally, it is important to note that no coal deposits had been formed at this time on Earth, precluding large amounts of metamorphic CO_2 release and suggesting that coal-derived metamorphic CO_2 might not play a dominant role in mass extinctions in general. This is also supported by observations from provinces associated with coal, like the Karoo or Parana traps, and not associated with any mass extinction.

Conclusions

In this study, we showed that the Kalkarindji large igneous province was emplaced at ca. 510-511 Ma using high precision $^{40}Ar/^{39}Ar$ and U-Pb mineral dating. These data can be

compared with zircon U-Pb ages from layers tightly bracketing the Early-Middle Cambrian boundary and showing the latter to be 510±1 Ma.

The temporal synchronicity between the eruption of and the Early-Middle Cambrian boundary at ~510 Ma is another example of a well-defined temporal correlation between volcanism, climate shifts and extinction and extends such a relationship to the beginning of the Phanerozoic Era. The likely factors responsible for the EMC extinction are climate shifts due to emission of mantle gases (SO_2 and possibly CO_2) dissolved in the magma, or gases (in particular CH_4 and SO_2) generated by the interaction between magma and evaporite layers and/or oil-rich rocks. CO_2 degassing due to magma-coal interaction may play a secondary role in biotic turnovers.

References

Alvarez, L.W., Alvarez W., Asaro, F., Michel, H.V., 1980, Extraterrestrial cause for the Cretaceous-Tertiary extinction. Science, v. 208, p. 1095-1108.

Black, B.A., Elkins-Tanton, L.T., Rowe, M.C., Peate, I.U., 2012, Magnitude and consequences of volatile release from the Siberian Traps: Earth and Planetary Science Letters, v. 317-318, p. 363-373.

Bradshaw, M.T., Bradshaw, J., Murray, A.P., Needham, D.J., Spencer, L., Summons, R.E., Wilmot, J., Winn, S., 1994, Petroleum Systems in West Australian Basins. In: P.G Purcell. & R.R. Purcell (Eds). The Sedimentary Basins of Western Australia: Proceedings of Petroleum Exploration Society of Australia Symposium, Perth, pp. 93-118.

Bryan, S.E., Ernst, R.E., 2008, Revised definition of Large Igneous Provinces (LIPs): Earth-Science Reviews, v. 86, p. 175-202.

249 Cohen, K.M., Finney, S.M., Gibbard, P.L., and Fan, J.-X., 2013. The ICS International
250 Chronostratigraphic Chart. Episodes, 36(3): 199-204.
251 Courtillot, V.E. and Renne, P.R., 2003, On the ages of flood basalt events: Comptes-Rendus des
252 Geosciences, v. 335, p. 113-140.
253 Courtillot, V., Kravchinsky, V.A., Quidelleur, X., Renne, P.R., Gladkochub, D.P., 2010,
254 Preliminary dating of the Viluy traps (Eastern Siberia): Eruption at the time of Late Devonian
255 extinction events?: Earth and Planetary Science Letters, v. 300, p. 239-245.
256 Evins, L., Jourdan, F., Philips, D., 2009, The Cambrian Kalkarindji Large igneous province:
257 extent and characteristics based on new $^{40}Ar/^{39}Ar$ and geochemical data: Lithos, v. 110, p.
258 294-304.
259 Ganino, C. and Arndt, N.T., 2009, Climate changes caused by degassing of sediments during
260 the emplacement of large igneous provinces: Geology, v. 37, p. 323-326.
261 Glass. L.M. and Phillips, D., 2006, The Kalkarindji Continental Flood Basalt Province: A new
262 Large Igneous Province in Australia with possible links to end-Early Cambrian faunal
263 extinctions: Geology, v. 34, p. 461–464.
264 Gozalo, R., Alvarez, M.E.D., Gamez, J.A., Zhuravlev, A.Y., Bauluz, B., Subias, I., Martorell,
265 J.B.C., Mayoral, E., Andres, H-j.J.A., Linan, E. 2013. Proposal of a reference section and
266 point for the Cambrian Series 2–3 boundary in the Mediterranean subprovince in Murero (NE
267 Spain) and its intercontinental correlation. Geological Journal, v. 48, p.142-155.
268 Harvey, T.H.P., Williams, M., Condon, D.J., Wilby, P.R., Siveter, D.J., Rushton, A.W.A., Leng,
269 M.J., Cabbott, S.E. 2011. A refined chronology for the Cambrian succession of southern
270 Britain. Journal of the Geological Society (London), v. 168, p. 705–716.

271 Hofmann, C., Féraud, G., Courtillot, V., 2000, $^{40}Ar/^{39}Ar$ dating of mineral separates and whole
272 rocks from the Western Ghats lava pile: further constraints on duration and age of the Deccan
273 traps. Earth and Planetary Sciences Letters, v. 180, p. 13-27.
274 Hough, M.L., Shields, G.A., Evins, L.Z, Strauss, H., Henderson, R.A. and Mackenzie, S., 2006,
275 A major sulphur isotope event at c. 510 Ma: a possible anoxia-extinction-volcanism
276 connection during the Early-Middle Cambrian transition?: Terra Nova, v. 18, p. 257-263
277 Jourdan, F., Reimold, U., Deutsch, A., 2012, Dating terrestrial impact structures. Elements, v. 8,
278 p.46-50.
279 Jourdan, F., Féraud, G., Bertrand, H., Watkeys, M.K., Renne, P.R., 2008, $^{40}Ar/^{39}Ar$ ages of the
280 sill complex of the Karoo large igneous province: implications for the Pliensbachian-Toarcian
281 climate change: G-cubed 9, Q06009, 20082008.
282 Keller, G., 2005, Impacts, volcanism and mass extinction: random coincidence or cause and
283 effect? Australian Journal of Earth Sciences, v. 52, p. 725 - 757
284 Landing, E., Bowring, S.A., Davidek, K.L., Westrop, S.R., Geyer, G. & Heldmaier, W., 1998,
285 Duration of the Early Cambrian: U–Pb ages of volcanic ashes from Avalon and Gondwana:
286 Canadian Journal of Earth Sciences, v. 35, p. 329–338.
287 Lindsay, J.F., 1987, Upper Proterozoic evaporites in the Amadeus basin, central Australia, and
288 their role in basin tectonics: GSA Bulletin, v. 99, p. 852-865.
289 Macdonald, F. A., Wingate, M. T. D., Mitchell, K., 2005, Geology and age of the Glikson
290 impact structure, Western Australia: Australian Journal of Earth Sciences, v. 52, p. 641-651.
291 Marzoli, A., Renne, P.R., Piccirillo, E.M., Ernesto, M., Bellieni, G., De Min, A., 1999,
292 Extensive 200-million-year-old continental flood basalts of the Central Atlantic Magmatic
293 Province: Science, v. 284, p. 616–618.

294 Montañez, I., Osleger, D., Banner, J.L., Mack, L.E., Musgrove, M., 2000, Evolution of Sr and C
295 isotope composition of Cambrian oceans: GSA Today, v. 10, p. 1–5.
296 Mundil, R., Ludwig, K.R., Metcalfe, I., Renne, P.R., 2004, Age and timing of the Permian mass
297 extinctions: U/Pb dating of closed-system zircons: Science, v. 305, p. 1760-1763.
298 Renne, P.R., Balco, G., Ludwig, K.R., Mundil, R., Min, K., 2011, Response to the comment by
299 W.H. Schwarz et al. on "joint determination of ^{40}K decay constants and ^{40}K*/^{40}K for the Fish
300 Canyon sanidine standard, and improved accuracy for ^{40}Ar/^{39}Ar geochronology" by P.R.
301 Renne et al. (2010): Geochimica Cosmochimica Acta, v. 75, p. 5097-5100.
302 Self, S., Thordarson, T., Widdowson, M., 2005, Gas Fluxes from Flood Basalt Eruptions:
303 Elements, v. 1, p. 283-287.
304 Sepkoski, J.J.JR, 1996, Patterns of Phanerozoic extinction: a perspective from global data bases.
305 In: Walliser O. H. ed. Global Events and Event Stratigraphy, pp. 35 – 52. Springer-Verlag,
306 Berlin.
307 Sobolev, S.V., Sobolev, A.V., Kuzmin, D.V., Krivolutskaya, N.A., Petrunin, A.G., Arndt, N.T.,
308 Radko, V.A., Vasiliev, Y.R., 2011, Linking mantle plumes, large igneous provinces and
309 environmental catastrophes: Nature, v. 477, p. 312-316.
310 Svensen, H., Planke, S., Polozov, A.G., Schmidbauer, N., Corfu, F., Podladchikov, Y.Y.,
311 Jamtveit, B., 2009, Siberian gas venting and the end-Permian environmental crisis: Earth and
312 Planetary Science Letters, v. 277, p. 490-500.
313 Wignall, P., 2005, The link between large igneous province eruptions and mass extinction.
314 Elements, v. 1, p. 293-297.
315 Zhuravlev, A.Y., Wood, R.A., 1996, Anoxia as the cause of the mid-Early Cambrian
316 (Botomian) extinction event: Geology, v. 24, p. 311-314.
317

341

342 [1]GSA Data Repository item 2009xxx, [including **Sample description, Analytical method,**

343 **Analytical results and Supplementary text]** is available online at

344 www.geosociety.org/pubs/ft2009.htm, or on request from editing@geosociety.org or Documents

345 Secretary, GSA, P.O. Box 9140, Boulder, CO 80301, USA.

Figure 1

Click here to download Figure: Fig1 General map.pdf

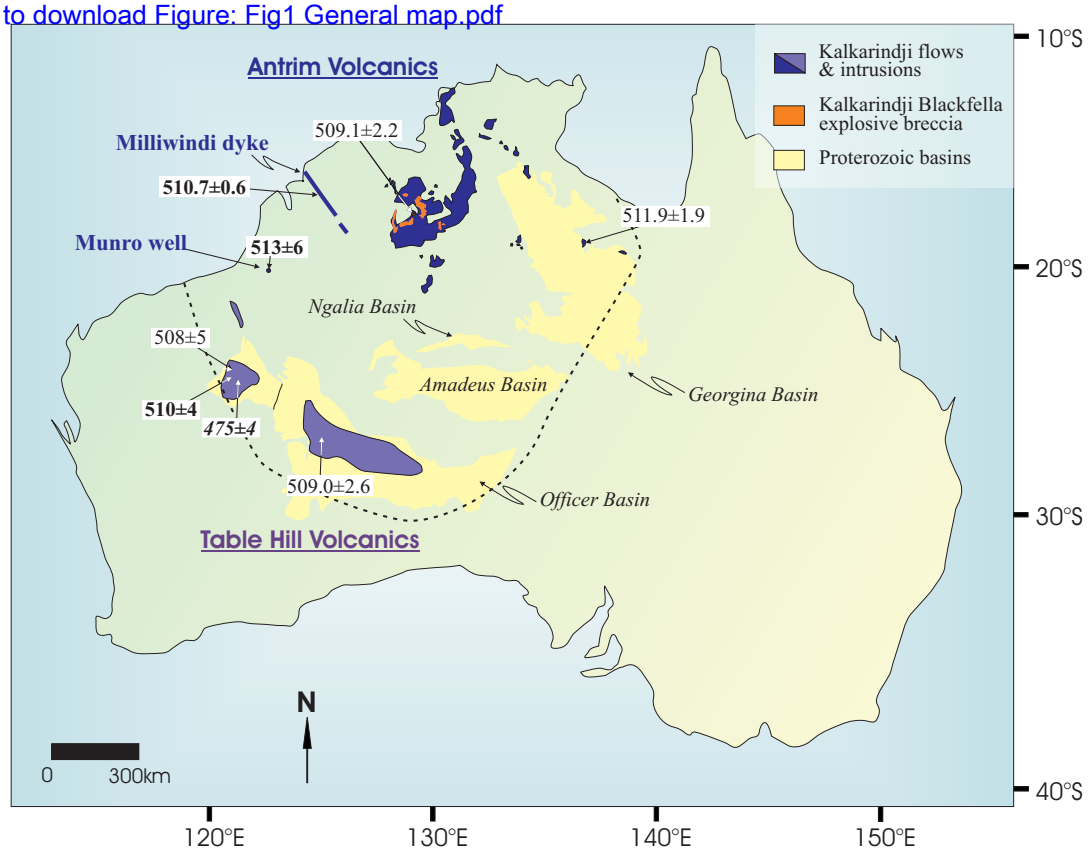

Fig. 1: Jourdan et al.

Figure 2
Click here to download Figure: Fig2 Mean ages.pdf

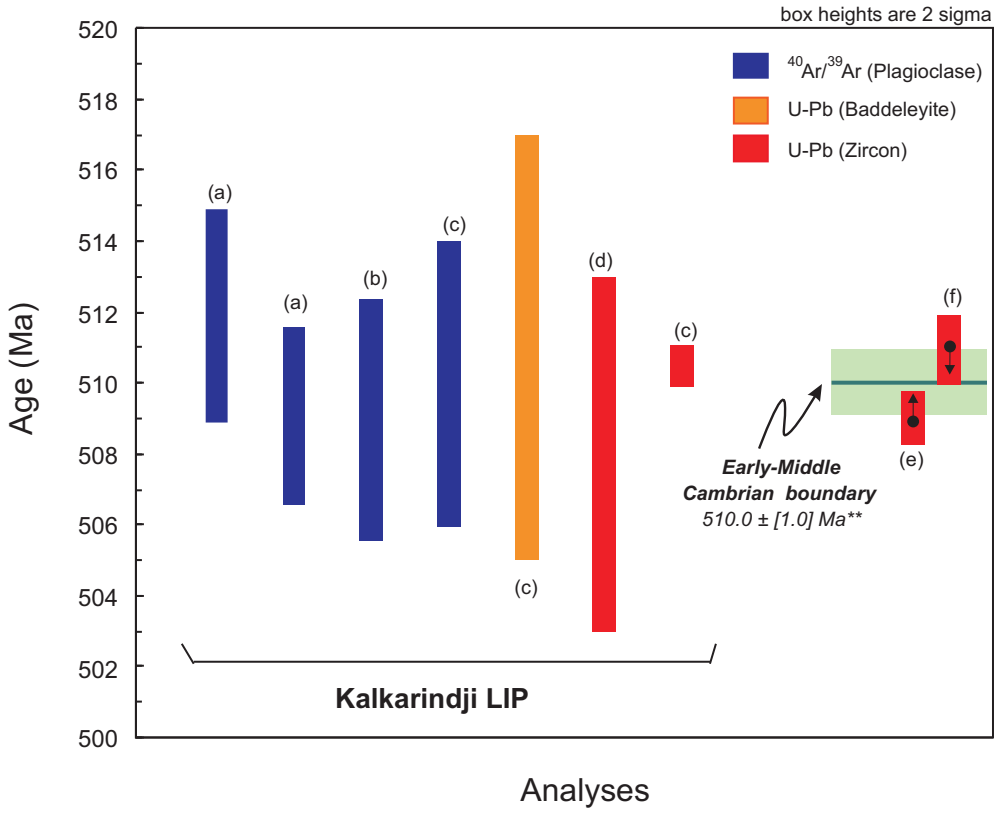

Fig.2: Jourdan et al.

Figure 3
Click here to download Figure: Fig3 CFB-extinction B&W.pdf

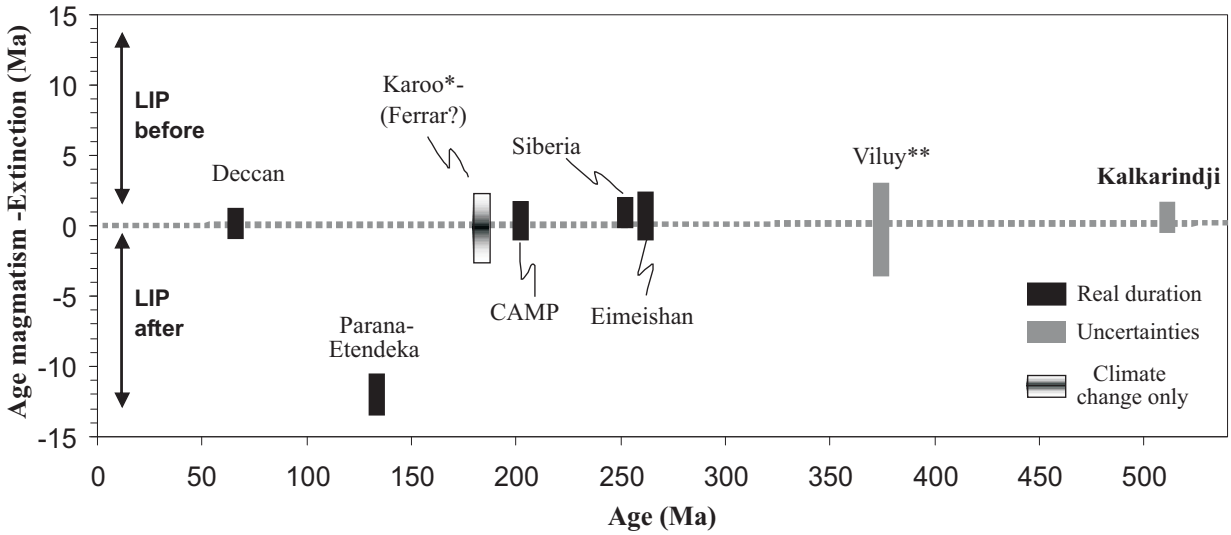

Fig. 3: Jourdan et al.

Supplementary Materials:

Material and methods

1. Sample descriptions

1.1 Milliwindi dolerite dyke

Sample Z01 consists of seven zircons that vary between 150 μm and 400 μm in length and appear to be unzoned (Fig. S1). These zircons were extracted from the original SHRIMP sample mount analysed by Hanley and Wingate (2000). The original sample was taken from a fresh surface exposure of the Milliwindi dyke which, although discontinuous, can be traced for at least 200 km (1). Petrographic analysis by (1) revealed that the sample is a coarse-grained dolerite consisting primarily of plagioclase, augite, and pigeonite, with minor ilmenite and apatite. Sample Z01 was also shown by these authors to be intimately associated with late-stage mineral assemblages, including alkali feldspars, quartz, biotite, and baddeleyite.

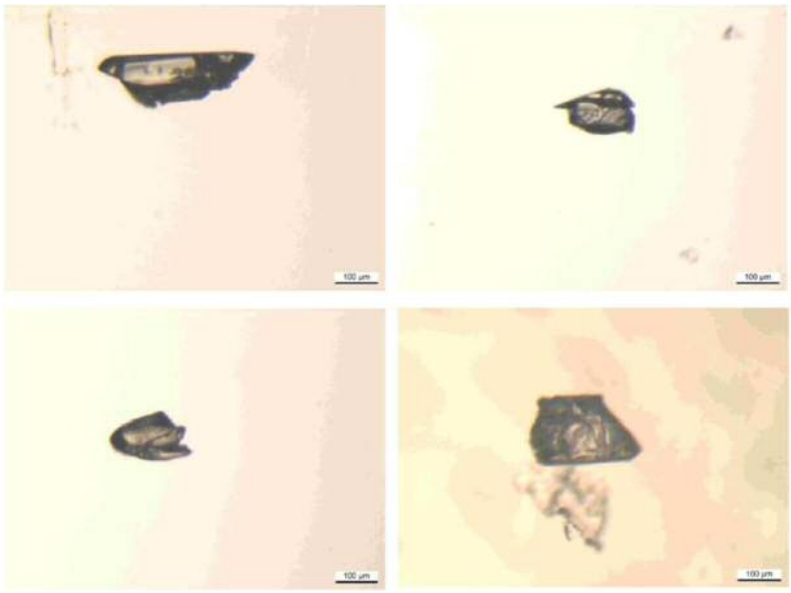

Fig. S1. Low resolution images of individual zircons from sample Z01.

1.2 Unnamed dyke, Canning basin.

Sample B01 was taken from petroleum exploration well Munro 1, drilled in the southern Canning basin. This hole penetrated a thick succession of Phanerozoic sediments before intersecting inferred Precambrian granitic basement at a depth of 2113.5 m (Fig. S2a). Sample B01 consists of 28 baddeleyite crystals that vary between 25 and 200 μm long (Fig. S2b). These grains are igneous in origin. The rock within which the mafic enclaves are hosted is characterised by micrographic intergrowths of orthoclase and quartz, making up approximately 70% of the rock (2) (Fig. S2a). Apatite, ilmenite, and chlorite (after plagioclase and biotite) are also present (2). It is possible that the mafic enclaves were derived from earlier erupted basalt that have been trapped in the intrusive rock, which represents the differentiated center of a thick dolerite sill.

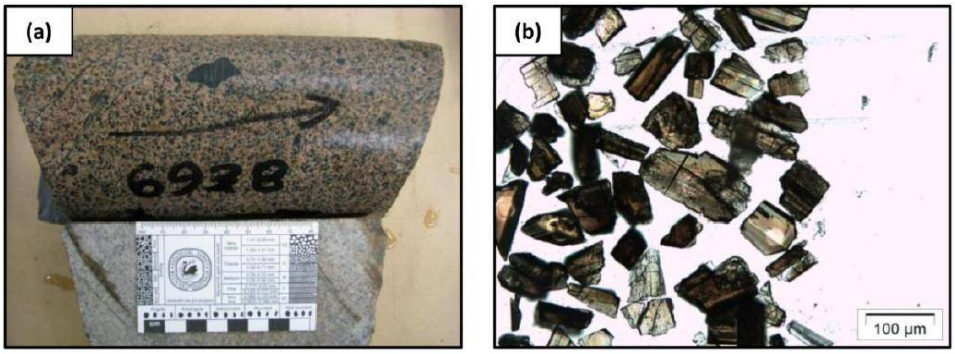

Fig. S2*: Images of sample B01. (a) Mafic enclaves within an alkaline syenite. (b) Separated crystals including many baddeleyite that may originate from the intrusive rock, the mafic enclaves, or both.*

1.3 Table Hill Volcanics

Sample 028 (Fig. S3) of the Table Hill Volcanics was collected from drillcore 09THD-028 over a depth interval of 65.5–66.0 m (Fig. S4). The dolerite sill continues undivided to a depth of 87.5 m. The base of the sill exhibits a chilled margin and is inter-fingered with the underlying sediments of the Boondawari Formation. From hand-sample observations, sample 028 exhibits a subophitic texture, characterized by clinopyroxene (augite), plagioclase, and magnetite. Chlorite and actinolite alteration gives the sample a mottled green appearance. Thin-section analysis of the nearby Boondawari and Akubra sills by (3) outlined the presence of brown–green hornblende, sericite, and chlorite, which replace labradorite and augite. The presence of these alteration minerals suggests sills within this area underwent greenschist metamorphism, possibly in relation to uplift within the Savory area of the northwest Officer Basin.

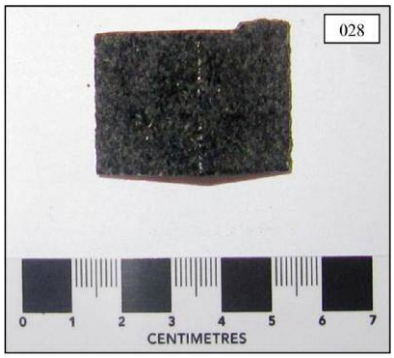

Fig. S3*: Hand sample photograph of sample 028.*

Sample 002 (Fig. S5) of the Table Hill Volcanics was sampled from drillcore 07THD-002 over a depth interval of 95.75–96.1 m. This dolerite sill continues undivided to a depth of 172.95 m. A chilled margin is observed with a sharp, angular contact against underlying diamictite. Sample 002 exhibits a subophitic texture, characterised by clinopyroxene (augite), cloudy (sericitized) plagioclase, and transparent plagioclase (Fig. S5). Minor hornblende, chlorite, and magnetite are also observed.

Fig. S4*: Core-tray photographs of drillcore 09THD-028. A chilled margin and interfingering with sediments of the Boondawari Formation can be observed.*

Fig. S5*: Hand-sample photograph of sample 002. Note the relatively fresh plagioclase amongst more altered (white) plagioclase.*

Melt inclusions

Melt inclusions are melt pockets a few micrometers in diameter that can retain the composition of the magma at the time of entrapment (i.e. pre-differentiation). It is assumed that they can thus provide indication on the amount of volatiles contained in the magma. Details about the significance of melt inclusions are summarized by (4).

We analyzed the composition of melt inclusions from 100-300 µm plagioclase crystals from sample EMP255. Plagioclase crystals from this sample have been used by (5) to carry out $^{40}Ar/^{39}Ar$ dating of the Table Hill Volcanics. The mini-plateau obtained for this sample indicates that some of the plagioclase crystals are fresh and can be used for melt inclusion S analyses. Plagioclase crystals from this sample were observed to contain numerous melt inclusions and individual crystals were carefully selected based on their freshness and melt inclusion contents.

Whole rocks

372 whole-rock samples have been recovered from 15 boreholes that intersected the Table Hills Volcanics. S and MgO analyses have been obtained at the analytical company Genalysis (Perth, Australia) by AusQuest Limited, a publically listed Australian exploration company. Data and sample locations have been made available for publication in this study (Table S4) based on an unpublished internal report by the company (6).

2. Analytical methods

2.1 U-Pb CA-TIMS (zircon)

Zircon crystals were extracted from the original SHRIMP sample mount from which (1) determined an imprecise SHRIMP U-Pb date of 513 ± 12 Ma. They were selected by hand in reflected light under a binocular microscope. Sample sizes were small, thus all zircons were selected for analysis. To minimize potential discordance due to Pb loss, all crystals were annealed in quartz crucibles at 900ºC for at least 72 hours and then leached in in Savillex PFA beakers for 12-16 hours in concentrated HF and a trace amount of HNO_3 at 180ºC. After leaching, the remaining zircons were cleaned with ultra-pure reagents (HCl, HNO3, and H2O) for several iterations using a hotplate and ultrasonic bath. Each crystal was carefully photographed and transferred to PFA microcapsules with the addition of several drops of HF and a weighed amount of (approximately 0.004 to 0.006 grams) isotopic tracer. The tracer is composed of ^{202}Pb-^{205}Pb-^{233}U-^{235}U and was prepared by the EARTHTIME organization. Microcapsules were then place inside a Parr bomb with a moat of seven millilitres of concentrated HF and trace amount of HNO3. The zircons were dissolved for no less than 72 hours at 210ºC. After dissolution, the samples were dried down on a hotplate within a clean laminar-flow hood and returned to the oven with 6 N HCl. The samples were dried again and

3 N HCl was added prior to single-column anion exchange chemistry (see Krogh, 1973) where U and Pb were collected in the same PFA beaker. The separated U and Pb were dried down with a drop of H_3PO_4 and loaded onto single Re filaments with a silica gel (7).

Analysis of U and Pb was performed on a Thermo-Finnegan Triton thermal ionization mass spectrometer at the University of Geneva. First, Pb was measured in dynamic mode using the secondary electron multiplier for at least 100 cycles. Next, U was typically measured for at least 200 cycles as an oxide in static mode with Faraday cups (10^{12} ohms). A few samples had low U concentrations that necessitated the use of the SEM in dynamic mode. Regular measurements of NBS 981 glass and a synthetic zircon solution of known composition were made so that various machine parameters, such as dead-time, linearity, and yield, could be monitored. Mass 203.5 accounted for baseline for Pb with interferences monitored by masses 202 and 205. The ratio of $^{202}Pb/^{205}Pb$ for the tracer is 0.99989. Mass fractionation corrections for U were made using a sample ratio for $^{238}U/^{235}U$ of 137.88. Pb blanks were monitored by periodically performing total procedural blank measurements and regular measurements of lead concentrations in reagents (table S1) .

All U-Pb zircon data were reduced using Tripoli software, and U-Pb zircon ages were calculated using U-Pb_Redux, version 2.60.042 (8). Isotopic ratios were reduced using two-sigma outlier rejection in Tripoli.

2.2 U-Pb TIMS (Baddeleyite)

Baddeleyite was separated using a Wilfley water-shaking table and hand-picked under a binocular microscope. Grains were transferred into Teflon dissolution bombs and washed successively with 2-3 N nitric acid and water. A small amount of $^{236-233}U$-^{205}Pb tracer solution was added before the sample was completely dissolved in $HF:HNO_3$ (10:1) at 210°C over 3

days. U and Pb were loaded together on an outgassed Re filament and measured in a Thermo Scientific Triton thermal ionisation multicollector mass spectrometer at the Museum of Natural History in Stockholm. The intensities of ^{207}Pb, ^{206}Pb, ^{205}Pb, and ^{204}Pb were measured in dynamic (peak-switching) mode in an ion counter equipped with RPQ filter. Typical filament temperatures were 1190-1230 °C for Pb and 1260-1300 °C for U. Fractionation-corrected U isotopic ratios were determined by monitoring the deviation in $^{233}U/^{236}U$ from that in the tracer solution (close to unity). The model composition of (9) was used to correct for initial common Pb, and total Pb and U blank were determined at 1 and 0.1 pg, respectively. The mass discrimination correction of Pb is constant at 0.1 ± 0.04 % per atomic mass unit. Decay constants used are from (10). Data reduction was performed using an in-house program written in Microsoft Excel (Per-Olof Persson, Stockholm) with algorithms from (11). Analytical results have been calculated and plotted using Isoplot (11).

2.3 $^{40}Ar/^{39}Ar$ (plagioclase)

Weathered edges of selected samples were removed by a diamond-blade saw. The remainder of the sample was cut into smaller fragments to pass more easily through a jaw crusher. A bucket was used to collect crushed fragments of the sample. The bucket and jaw crusher were thoroughly cleaned between each sample using pressurized air and a damp cloth. The metal plates of the crusher were rigorously scrubbed with an array of wire brushes to prevent cross-contamination between samples. Each sample was then crushed and milled using a tungsten carbide ring mill. The mill was activated on short bursts between 4 to 8 seconds to prevent grains from becoming completely pulverised. The milled sample was passed through two sieves with mesh sizes of 250 and 125 µm. Sample remaining above the 250 µm mesh was re-milled, material between 250 and 125 µm was retained for analysis, and below 125 µm stored

aside as waste pulp. The 125–250 μm size fraction of each sample was washed to remove any fine powder. Samples were washed with water and allowed to settle briefly before expelling the water. Once the water expelled became clear, samples were placed in an ultrasonic bath to remove any remaining fines. Samples were rinsed in ethanol and dried under a heat lamp. Plagioclase was separated using a Frantz magnetic separator. A vertical angle of 35° was used on the first few runs with low magnetic fields to remove the highly magnetic fraction. This angle was reduced to 20° with the magnetic field increased slightly on each consecutive run. Towards the end, when predominantly plagioclase is left, the vertical and horizontal angles are both lowered in order to remove the heavily altered grains. Plagioclase grains were then hand-picked using a binocular microscope. Only the most optically transparent grains were selected, and grains that showed any sign of sericite alteration (cloudiness) or fractures and cracks that could host sericite were eliminated. Any grains hosting inclusions internally or on grain edges were also eliminated. Each sample underwent multiple screenings. Between 5 and 10 milligrams of plagioclase were isolated from each sample for analysis. Each sample was leached for 1 minute in dilute hydrofluoric acid before being thoroughly rinsed with distilled water in an ultrasonic cleaner.

The two Antrim Plateau and Table Hill samples were loaded into the separate large wells of a 1.9 cm wide by 0.3 cm deep aluminum disc. These wells were bracketed by small wells that included Hb3gr (standard), used as a neutron fluence monitor for which a good in-between grain reproducibility has been demonstrated (12) and an age of 1080.4 ± 1.1 Ma (1σ) based on the R-value of (13) has been adopted (14). The mean J-values computed from standard grains within the small pits range from 0.009481 ± 0.0000137 (0.145%) to 0.00968 ± 0.0000203 (0.21%), determined as the average and standard deviation of J-values of the small wells for each irradiation disc. Mass discrimination was monitored using an automated air

pipette and provided a range in mean values of 1.005337 ± 0.0025 to 1.005447 ± 0.0034 per dalton (atomic mass unit) relative to an air ratio of 298.56 ± 0.31 (Lee et al. 2006). The correction factors for interfering isotopes were $(^{39}Ar/^{37}Ar)_{Ca}$ = 7.30x10^{-4} (± 11%), $(^{36}Ar/^{37}Ar)_{Ca}$ = 2.82x10^{-4} (± 1%) and $(^{40}Ar/^{39}Ar)K$ = 6.76x10^{-4} (± 32%). The $^{40}Ar/^{39}Ar$ analyses were performed at the Western Australian Argon Isotope Facility at Curtin University, operated by a consortium consisting of Curtin University and the University of Western Australia. Multi-grain aliquots were wrapped in zero-blank niobium foil and step-heated using a 110 W Spectron Laser Systems, with a continuous Nd-YAG (IR; 1064 nm) laser rastered over the sample for 1 minute to ensure a homogenously distributed temperature. The gas was purified in a stainless steel extraction line using three SAES AP10 getters and a liquid nitrogen condensation trap. Ar isotopes were measured in static mode using a MAP 215-50 mass spectrometer (resolution of ~500; sensitivity of 4x10^{-14} mol/V) with a Balzers SEV 217 electron multiplier mostly using 9 to 10 cycles of peak-hopping. Data acquisition was performed with the Argus program written by M.O. McWilliams and running within a Labview environment. Raw data were processed using the ArArCALC software (15) and ages calculated using decay constants recommended by (14). Blanks were monitored every 3 to 4 steps and typical ^{40}Ar blanks range from 1 x 10-16 to 2 x 10-16 mol. Ar isotopic data are corrected for blank, mass discrimination, and radioactive decay. Individual uncertainties are reported at the 1σ level unless otherwise indicated. Our criteria for the determination of a plateau are as follows: 1. plateaus must include at least 70% of ^{39}Ar, 2. the plateau should be distributed over a minimum of 3 consecutive steps agreeing at 95% confidence level and satisfying a probability of fit (P) of at least 0.05. Plateau ages are reported at the 2σ level and are calculated using the mean of all the plateau steps, each weighted by the inverse variance of their individual analytical uncertainty. Integrated ages (2σ) are calculated using the total

gas released for each Ar isotope. Inverse isochrons include the maximum number of steps with a probability of fit ≥ 0.05. All sources of uncertainties are included in calculations.

2.4 Melt inclusions S and MgO analyses in plagioclase

Selected grains were carefully documented using optical microscopy. The melt inclusions were all devitrified and/or crystallized and contained water as was observed using infrared spectroscopy (FTIR). In order to quantify the volatile content, the inclusions required homogenisation. The furnace homogenization experiments involved placing the grains in platinum foil packets, which were hoisted up into the furnace and heated to required temperature, and then quenched by dropping the foil packet in cold water. A step-wise heating schedule was employed to quench the inclusions as close to the homogenisation temperature as possible. The quenched inclusions were then analysed with FTIR for determining the water content. However, due to apparent water loss during the homogenisation experiments (no water signal after homogenisation), the FTIR spectroscopy was abandoned in favour of elemental analysis by electron microscopy (EMPA). Plagioclase grains were mounted and polished until the inclusions were exposed. Devitrified and homogenised inclusions were analysed by with the Cameca SX50 EMPA at Uppsala University in March 2009. We used 20 Kv voltage and a 15 nA current, and a beam size of ca. 1 μm. Twelve elements were analyzed simultaneously (F, Na, Mg, Al, Si, Cl, K, Ca, Ti, S, Mn, Fe). The instrument was calibrated using natural and synthetic standards, and raw data were ZAF-corrected. The detection limit for S was ca 250 μg/g.

2.5 Whole rocks S and MgO analyses

MgO and S contents were analyzed by Inductively Coupled Plasma Optical Emission Spectrometry (ICP-OES) at the analytical company Genalysis (Perth, Australia) by AusQuest Limited, a publically listed Australian exploration company.Precision on major elements and trace elements are ±3% or better and ±10% or better, respectively.

3. Analytical results

3.1 Zircons from Milliwindi dolerite dyke

Low-resolution photos (Fig. S1) show the seven zircons of sample Z01. All individual zircon analyses are plotted on a Concordia diagram (Fig. S6). Analysis Z7 appears to reflect minor loss of radiogenic Pb loss and was not used in age calculations. The remaining six zircons form a cluster on the Concordia plot (Fig. S6a; Table S1) and define a $^{206}Pb/^{238}U$ age trend (Fig. S6, inset) between 511.23 ± 0.43 [0.70] Ma for Z3, to 510.72 ± 0.42 [0.69] Ma for Z2. Five zircons produce a concordant $^{206}Pb/^{238}U$ weighted mean age of **510.67 ± 0.30 [0.62] Ma** (Figure S6). This population is statistically concordant with a MSWD and P-values of 2.0 0.09. Although other mean ages can be calculated by selecting different zircons (e.g., Z4, Z5, Z6, Z2 only; 510.52 ± 0.32 [0.63] Ma; P=0.49), the difference is within uncertainty and we believe these five results best represent the age of the Milliwindi dyke. The slightly older ages indicated by Z1 and Z3 are believed to represent antecrysts – zircons that have crystallised within the magma chamber up to a few hundred thousand years prior to the emplacement of the dyke. Therefore, the results from five consecutive zircons (red analyses in Fig. S6) are taken to represent the true emplacement age of the Milliwindi dyke.

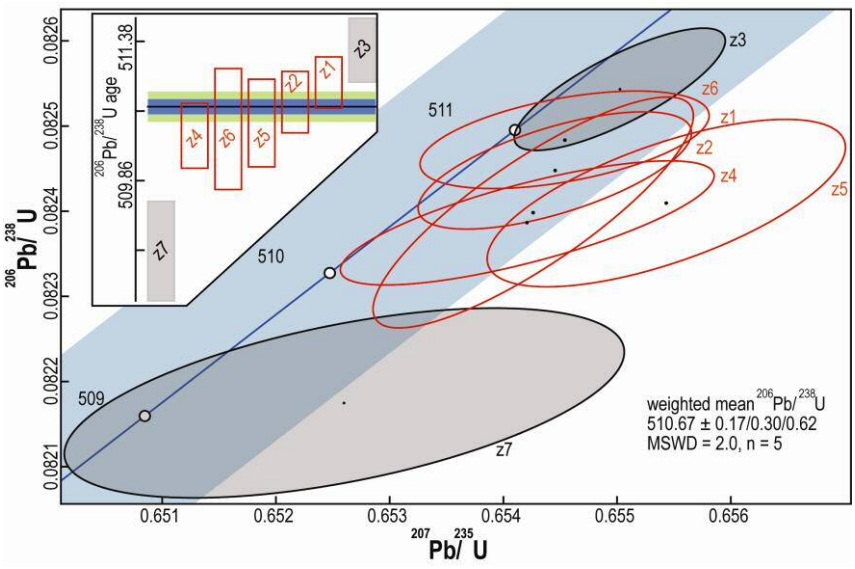

Fig. S6. *Analytical data for single zircons from sample Z01. (a)* $^{206}Pb/^{238}U$ *and* $^{207}Pb/^{235}U$ *ratios in zircons of sample Z01. Note the concordance of six zircons. Red ellipses in the concordia diagram indicate analyses used in the age calculation; blue line is the concordia curve including uncertainties. Weighted mean age uncertainties are indicated as analytical/including tracers/all source of uncertainties. (b)* $^{206}Pb/^{238}U$ *dates for single-grains zircons. R; red boxes indicate dates included in the age calculation; Grey boxes outline zircons not used in age calculation. Blue bar show analytical uncertainties and green bar show all source of uncertainties on the weighted mean age.*

	Composition			Isotopic Ratios											Dates (Ma)						
Frac-	Th	Pb*	Pb*	^{206}Pb	^{208}Pb	^{207}Pb	±2σ	^{206}Pb	±2σ	^{207}Pb	±2σ	^{238}U		Corr.	^{207}Pb	±2σ	^{207}Pb	±2σ	^{238}U	±2σ
tion	U_a	Pb_{cb}	$(pg)_c$	$^{204}Pb_d$	$^{206}Pb_e$	$^{206}Pb_e$	%	$^{238}U_e$	%	$^{235}U_e$	%	$<Th>_{ef}$	±2σ %	coef.	$^{206}Pb_g$	abs	$^{235}U_g$	abs	$<Th>_f$	abs
z1	1.76	87	85.4	3928	0.548	0.057553	0.14	0.082484	0.057	0.6545	0.16	0.082493	0.057	0.497	512.8	3.1	511.27	0.64	510.99	0.28
z2	1.52	102	312	4875	0.474	0.057570	0.12	0.082448	0.068	0.65445	0.15	0.082458	0.068	0.646	513.4	2.6	511.22	0.60	510.78	0.34
z3	1.40	167	297	8147	0.435	0.057554	0.072	0.082543	0.071	0.65502	0.12	0.082554	0.071	0.793	512.8	1.6	511.57	0.46	511.35	0.35
z4	1.60	82	162	3824	0.498	0.057592	0.16	0.082386	0.072	0.6542	0.21	0.082396	0.072	0.757	514.3	3.5	511.07	0.82	510.41	0.35
z5	1.74	81	118	3703	0.544	0.057683	0.15	0.082410	0.097	0.6554	0.20	0.082419	0.097	0.666	517.7	3.3	511.82	0.79	510.55	0.48
z6	1.55	152	123	7163	0.484	0.057588	0.096	0.08240	0.13	0.6543	0.18	0.082409	0.13	0.838	514.1	2.1	511.10	0.71	510.49	0.66
z7	1.41	41	84.5	2016	0.441	0.05760	0.27	0.082175	0.11	0.6526	0.31	0.082186	0.11	0.537	514.5	5.8	510.1	1.2	509.16	0.54

a Th contents calculated from radiogenic ^{208}Pb and the $^{207}Pb/^{206}Pb$ date of the sample, assuming concordance between U-Th and Pb systems.
b Ratio of radiogenic Pb (including ^{208}Pb) to common Pb.
c Total mass of radiogenic Pb.
d Measured ratio corrected for fractionation and spike contribution only.
e Measured ratios corrected for fractionation, tracer and blank.
f Corrected for initial Th/U disequilibrium using radiogenic ^{208}Pb and Th/U[magma] = 4.
g Isotopic dates calculated using the decay constants λ_{238} = 1.55125E-10 and λ_{235} = 9.8485E-10 (Jaffey et al. 1971).

***Table S1**: U-Pb analytical data for zircons from sample Z01.*

3.2 Baddeleyite from Canning Basin basement intrusion

Six analyses (Bd-A to Bd-F) were conducted using U–Pb TIMS. Variable discordance is attributed to geologically-recent Pb loss. Analyses Bd-B, Bd-C, and Bd-E are in good agreement at ~500 Ma (Fig. S7) and collectively account for 17 of the total 28 grains. Analyses show the occurrence of between 6 and 36 % of common lead. Regression of the five analyses, aligned with a forced lower intersection of 0 ± 100 Ma, yields an upper intercept age of 513 ± 4 [6] Ma (MSWD = 1.5; P=0.21). Note that when using a non-anchored lower intercept of -72 ± 140 Ma, we calculate an indistinguishable age of 511 ± 4 [5] Ma (MSWD = 1.6; P = 0.20) taken to represent the crystallization age of the sample. Analyses Bd-D and Bd-F yield slightly younger results and presumably reflect minor loss of radiogenic Pb. Group Bd-A, which yields an older discordant result, contained eight grains and, given that baddeleyite inheritance is very unlikely, may have included material that was not baddeleyite, but contained a small amount of Pb. Groups Bd-A, Bd-D, and Bd-F were not used in age calculation.

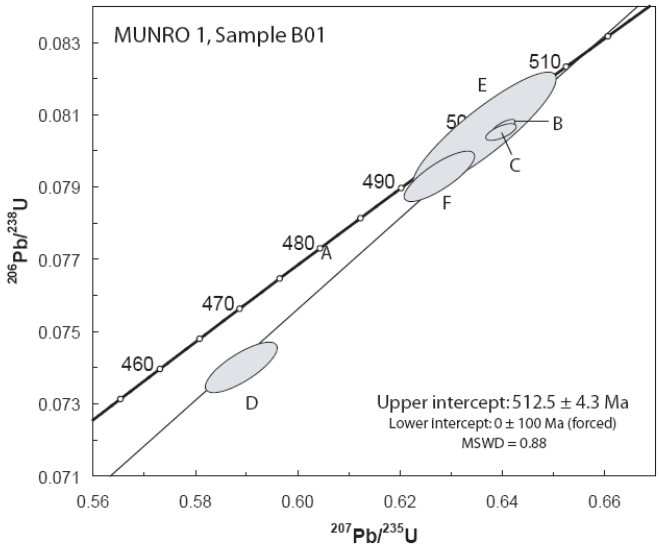

Fig. S7*: Analytical data for baddeleyite fractions (Bd-B–F) from sample B01. The concordia curve is shown with circles every 10 Ma; error ellipses are ±2 sigma. The result for fraction Bd-A is not shown. The upper intercept age is based on a discordia regression through 5 analyses (excluding Bd-A).*

Analysis no. (number of grains)	U/ Th	Pbc/ Pbtot[1)]	^{206}Pb/ ^{204}Pb raw[2)]	^{207}Pb/ ^{235}U	± 2s % err	^{206}Pb/ ^{238}U [corr][3)]	± 2s % err	^{207}Pb/ ^{235}U	^{206}Pb/ ^{238}U	^{207}Pb/ ^{206}Pb [age, Ma]	± 2s % err	Concord-ance
Bd-A (8 grains)	6.6	0.356	140.7	0.6981	1.06	0.08526	0.44	537.7	527.5	581.2	20.0	0.908
Bd-B (4 grains)	11.9	0.054	1219.5	0.6400	0.29	0.08067	0.20	502.3	500.1	512.3	4.3	0.976
Bd-C (11 grains)	8.0	0.096	649.9	0.6394	0.38	0.08052	0.24	502.0	499.2	514.5	6.3	0.970
Bd-D (3 grains)	5.8	0.230	250.4	0.5887	0.98	0.07398	0.77	470.0	460.1	518.9	13.7	0.887
Bd-E (2 grains)	7.2	0.205	308.9	0.6362	1.80	0.08055	1.66	499.9	499.4	502.5	18.5	0.994
Bd-F (5 grains)	13.9	0.055	1231.9	0.6274	0.90	0.07929	0.72	494.5	491.9	506.5	11.8	0.971

[1)] Pbc = common Pb; Pbtot = total Pb (radiogenic + blank + initial).

[2)] measured ratio, corrected for fractionation and spike.

[3)] isotopic ratios corrected for fractionation (0.1% per amu for Pb), spike contribution, blank (1 pg Pb and 0.1 pg U) and initial common Pb. Initial common Pb corrected with isotopic compositions from the model of Stacey and Kramers (1975) at the age of the sample.

Table S2*: U-Pb analytical data for Baddeleite from the Canning Basin intrustion.*

3.3. $^{40}Ar/^{39}Ar$ results (plagioclase)

Both samples from dolerite sills of the Table Hill Volcanics from the Officer Basin produced meaningful plateau ages (Fig. S8). The success of these samples compared with those from the Antrim Plateau Volcanics may relate to the relative abundance and coarse-grained nature of plagioclase within the dolerite sills. Samples 002 and 028 originate from drillholes 07THD-002 and 09THD-028 respectively. These holes are located ~65 km apart, and the two samples were taken from sills believed to be part of the Kalkarindji LIP. This is confirmed as both samples share the same major and trace element patterns. Sample 002 produced a plateau age of **510 ± 4 [4][1] Ma**, with 74% of total ^{39}Ar released (Fig. S8a). This age is statistically reliable (MSWD = 0.74; P value of 0.69), and believed to represent the emplacement age of the Kalkarindji sills in the Officer Basin. The first few steps (~28%) show minor signs of 40Ar diffusion, probably due to a minor thermal event, whereas the mid- to high-temperature steps define a plateau age of **510 ± 4 [4] Ma**.

The K/Ca plot for sample 002 shows a saddle-like shape with values around 0.02–0.03 (Ca/K ~30–50). Such shapes, when correlated with step-age variation, usually indicate the occurrence of sericite within the plagioclase. Here, no such correlation is observed, and the Ca/K variation is attributed to mineral zoning, Perthite exsolution, or the occurrence of minor syn-eruption sericite alteration. In any case, the age of **510 ± 4 [4] Ma** indicates the age of crystallisation within error. The data define significant spread along the inverse isochron, and yield an age of 507 ± 9 [10] Ma. This age is in agreement with the plateau age and $^{40}Ar/^{36}Ar$ intercept (307 ± 14), which is within the uncertainty of an atmospheric value.

[1] The systematic uncertainties represent and addition of ± 0.2 Ma (2σ) and have been calculated using the error propagation calculations of (14) and the R-value (FCs/Hb3gr) of (13).

Sample 028, from 09THD-028, produced a significantly younger plateau age of **475 ± 4 [4]**, with 94% of total 39Ar released (Fig. S8b). This date is statistically reliable (MSWD = 1.27; P = 0.21) yet significantly younger than that obtained from sample 002. The K/Ca plot exhibits a weak wave-like pattern but, most importantly, a K/Ca value of ~0.4–0.6 (Ca/K ~2), which is consistent with a strong sericitisation of plagioclase (usual observed Ca/K values ~20-150, e.g. (16) and numerous references within) and thus the plateau age probably indicates the age of a late hydrothermal alteration event. Sample 028 produced an isochron age of 471 ± 9 [9] Ma, with the majority of steps forming a tight grouping near the radiogenic Ar axis. This prevents a proper determination of the trapped Ar ratio, which is reflected by the uncertainty obtained (~320 ± 22). At face value, the approximate trapped Ar ratio falls within error of the atmospheric ratio. The slightly higher intercept, if significant, may result from excess Ar associated with the hydrothermal fluids responsible for the alteration event.

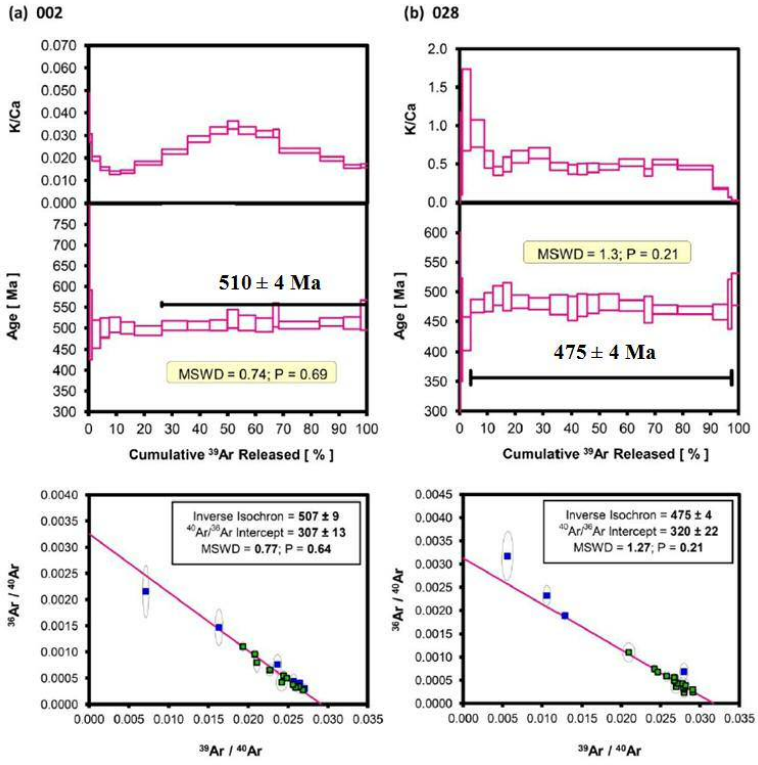

Fig S8: *$^{40}Ar/^{39}Ar$ plateau age and K/Ca spectra, and inverse isochron plots for samples 002 (a) and 028 (b) of the Table Hill Volcanics.*

Table S3A (Sample 002)

Relative Abundances			36Ar	%1σ	37Ar	%1σ	38Ar	%1σ	39Ar	%1σ	40Ar	%1σ	Age ± 2σ (Ma)	40Ar(r) (%)	39Ar(k) (%)	K/Ca ± 2σ
1A18042D	61.00 W		0.0000826	11.584	0.0027093	6.352	0.0001802	6.893	0.0002722	2.757	0.0379331	0.304	699.71 ± 247.23	35.65	0.21	0.0429 ± 0.0059
1A18043D	62.50 W		0.0001193	11.294	0.0188765	2.885	0.0001495	5.334	0.0012782	1.504	0.0775344	0.220	508.74 ± 83.19	56.11	0.99	0.0288 ± 0.0019
1A18044D	64.00 W		0.0001447	10.517	0.0827202	2.334	0.0001546	7.289	0.0038429	1.086	0.1597748	0.058	486.16 ± 32.78	77.33	2.97	0.0197 ± 0.0010
1A18046D	65.00 W		0.0001057	11.434	0.1196290	2.299	0.0000933	9.791	0.0043129	0.711	0.1643238	0.174	501.01 ± 23.19	86.93	3.31	0.0152 ± 0.0007
1A18047D	66.00 W		0.0001065	9.476	0.1597702	2.285	0.0000878	7.031	0.0050991	0.994	0.1893123	0.104	507.56 ± 18.26	90.31	3.91	0.0134 ± 0.0007
1A18049D	67.00 W		0.0001270	8.322	0.1998120	2.290	0.0001193	6.702	0.0066059	0.697	0.2388011	0.072	499.66 ± 14.38	91.17	5.07	0.0139 ± 0.0007
1A18051D	68.00 W		0.0002778	6.263	0.3046384	2.296	0.0002291	6.844	0.0127616	0.362	0.4736820	0.080	493.23 ± 11.46	87.90	9.84	0.0177 ± 0.0008
1A18052D	68.60 W		0.0001817	8.858	0.2207675	2.304	0.0001896	8.125	0.0118650	0.429	0.4356710	0.075	505.82 ± 11.42	91.82	9.18	0.0228 ± 0.0011
1A18053D	69.00 W		0.0001771	6.837	0.1562553	2.325	0.0001694	8.505	0.0104065	0.613	0.3912018	0.136	505.46 ± 10.76	89.85	8.07	0.0283 ± 0.0014
1A18054D	69.50 W		0.0002132	5.453	0.1085241	2.354	0.0001673	8.167	0.0082020	0.681	0.3325766	0.152	506.51 ± 12.75	83.61	6.37	0.0322 ± 0.0016
1A18057D	70.30 W		0.0001605	8.130	0.0614377	2.360	0.0000979	15.161	0.0050014	1.089	0.2183134	0.161	521.77 ± 22.54	80.42	3.89	0.0347 ± 0.0018
1A18058D	71.50 W		0.0004795	3.704	0.1052120	2.482	0.0002347	8.718	0.0079434	0.620	0.4071043	0.107	512.26 ± 18.31	67.01	6.17	0.0322 ± 0.0016
1A18059D	72.50 W		0.0003977	3.949	0.1116803	2.330	0.0002473	6.363	0.0080400	0.716	0.3823146	0.092	507.40 ± 16.58	71.40	6.24	0.0306 ± 0.0015
1A18061D	79.70 W		0.0000588	15.727	0.0385498	2.559	0.0000802	18.921	0.0027926	1.436	0.1142673	0.327	531.14 ± 28.96	87.47	2.17	0.0308 ± 0.0018
1A18062D	81.50 W		0.0004748	3.988	0.3460382	2.286	0.0007274	3.326	0.0189599	0.510	0.7533253	0.045	506.74 ± 9.20	85.05	14.67	0.0232 ± 0.0011
1A18063D	82.00 W		0.0002034	5.733	0.2383215	2.324	0.0005646	3.360	0.0110470	0.622	0.4191061	0.120	513.94 ± 10.25	90.30	8.53	0.0196 ± 0.0009
1A18064D	82.50 W		0.0001742	7.421	0.2088813	2.300	0.0003414	4.686	0.0080071	0.712	0.3065650	0.143	511.87 ± 14.47	88.77	6.16	0.0162 ± 0.0008
1A18066D	83.00 W		0.0001295	10.165	0.0744099	2.364	0.0001453	10.755	0.0029142	0.800	0.1357474	0.271	530.90 ± 36.01	76.13	2.24	0.0165 ± 0.0008

Table S3B (Sample 028)

Relative Abundances			36Ar	%1σ	37Ar	%1σ	38Ar	%1σ	39Ar	%1σ	40Ar	%1σ	Age ± 2σ (Ma)	40Ar(r) (%)	39Ar(k) (%)	K/Ca ± 2σ
1A18083D	61.00 W		0.0001169	8.055	0.0002656	125.231	0.0000818	11.155	0.0002071	5.633	0.0368017	2.496	151.27 ± 449.67	5.19	0.15	0.335 ± 0.840
1A18084D	62.50 W		0.0002595	4.698	0.0008700	41.945	0.0002338	4.917	0.0011876	2.164	0.1117068	0.834	436.58 ± 86.55	30.72	0.83	0.587 ± 0.493
1A18085D	64.00 W		0.0001051	13.309	0.0015217	22.081	0.0001000	7.890	0.0042584	0.759	0.1522414	0.612	429.93 ± 27.67	79.47	2.99	1.203 ± 0.532
1A18086D	65.00 W		0.0000588	15.455	0.0033530	9.934	0.0001023	10.735	0.0069833	0.420	0.2398283	0.384	475.90 ± 11.34	92.79	4.90	0.895 ± 0.178
1A18088D	65.50 W		0.0000520	15.794	0.0035219	10.211	0.0000580	13.376	0.0045690	0.630	0.1630869	0.570	482.45 ± 15.94	90.66	3.20	0.558 ± 0.114
1A18089D	66.00 W		0.0000442	22.113	0.0053776	7.079	0.0000751	12.846	0.0050952	0.592	0.1819338	0.524	493.56 ± 16.48	92.99	3.57	0.407 ± 0.058
1A18090D	66.70 W		0.0000566	19.722	0.0036241	9.535	0.0000578	13.697	0.0041581	1.086	0.1540088	0.618	491.44 ± 23.63	89.22	2.91	0.493 ± 0.095
1A18091D	67.70 W		0.0001006	9.321	0.0064736	6.659	0.0001252	11.587	0.0089380	0.823	0.3192195	0.305	483.14 ± 11.13	90.76	6.26	0.593 ± 0.080
1A18093D	68.60 W		0.0001372	7.559	0.0073859	5.360	0.0001870	5.431	0.0110060	0.722	0.3943904	0.239	479.92 ± 9.82	89.77	7.71	0.640 ± 0.069
1A18094D	69.20 W		0.0001395	10.540	0.0080209	5.347	0.0001453	7.853	0.0087055	1.164	0.3197818	0.309	478.11 ± 16.72	87.18	6.10	0.466 ± 0.051
1A18095D	69.70 W		0.0000978	11.618	0.0049843	6.954	0.0000950	9.409	0.0049606	0.967	0.1852526	0.505	471.75 ± 20.33	84.46	3.48	0.428 ± 0.060
1A18096D	70.20 W		0.0001148	9.729	0.0049283	8.251	0.0001049	11.495	0.0049508	0.592	0.1921256	0.481	477.39 ± 19.00	82.38	3.47	0.432 ± 0.071
1A18098D	71.00 W		0.0001865	5.767	0.0057421	6.589	0.0001428	6.200	0.0060064	0.679	0.2481014	0.387	479.32 ± 15.70	77.75	4.21	0.449 ± 0.060
1A18099D	72.00 W		0.0002888	5.896	0.0097023	4.285	0.0002232	4.890	0.0103980	0.583	0.4219476	0.235	482.55 ± 13.94	79.75	7.29	0.461 ± 0.040
1A18100D	72.80 W		0.0002404	5.399	0.0107615	4.695	0.0002618	5.173	0.0129776	0.501	0.4849264	0.207	476.51 ± 9.12	85.39	9.10	0.518 ± 0.049
1A18103D	79.60 W		0.0000642	15.061	0.0045424	5.699	0.0000858	10.140	0.0041053	1.460	0.1476229	0.298	469.72 ± 22.30	87.27	2.88	0.388 ± 0.046
1A18104D	80.80 W		0.0001785	5.783	0.0105758	3.260	0.0002469	3.550	0.0128965	0.458	0.4575240	0.109	470.03 ± 7.42	88.55	9.04	0.524 ± 0.035
1A18105D	81.50 W		0.0001903	6.516	0.0173060	2.876	0.0003455	3.176	0.0181797	0.475	0.6247766	0.069	468.85 ± 6.68	91.14	12.74	0.451 ± 0.026
1A18106D	82.00 W		0.0001687	6.803	0.0186398	2.635	0.0002351	3.845	0.0077739	0.668	0.2902559	0.109	465.87 ± 12.93	83.19	5.44	0.179 ± 0.010
1A18108D	82.50 W		0.0001008	9.074	0.0123932	3.473	0.0001013	11.987	0.0018633	1.849	0.0885586	0.366	478.82 ± 41.87	67.21	1.30	0.064 ± 0.005
1A18109D	83.00 W		0.0005339	2.202	0.0746873	2.442	0.0007611	2.140	0.0035388	0.728	0.2716778	0.122	504.00 ± 27.03	43.65	2.44	0.020 ± 0.001

Table S3. $^{40}Ar/^{39}Ar$ data summary. Relative abundance values are corrected for mass discrimination, blanks, and radioactive decay. Measurement uncertainties are given at the 1σ level. **A.** Sample 002, **B.** sample 028.

3.4. S and MgO of plagioclase melt inclusions

Data from 8 inclusions, that were glassy after quenching, are presented in Table S5 and Fig. S9. S content varies from 0 to 1254 μm/g and is uncorrelated to MgO which varies

from 6.2 to 2.8 wt%. A S content of 0 µg/g is associated with cracks in the minerals and likely indicate degassing during mineral preparation or heating.

Inclusion ID	TiO2 (wt%)	FeO (wt%)	MgO (wt%)	S (µg/g)
1165_9	1.06	12.18	4.9	1254
1165_15	1.1	10.5	4.1	913
1165_15b	*1.1*	*13.0*	*5.4*	*0*
1185_6	0.8	5.7	4.3	113
1185_3	0.8	9.7	6.2	830
1185_3b	0.6	10.1	5.9	840
1193_O	*0.8*	*5.2*	*2.8*	*0*
1190_2	0.6	6.1	4.6	310

Table S4. *EMPA data (Uppsala) of glassy inclusions from sample EMP255 (see sample description and $^{40}Ar/^{39}Ar$ data in (5). Inclusions with S loss due to cracks are indicated in italics.*

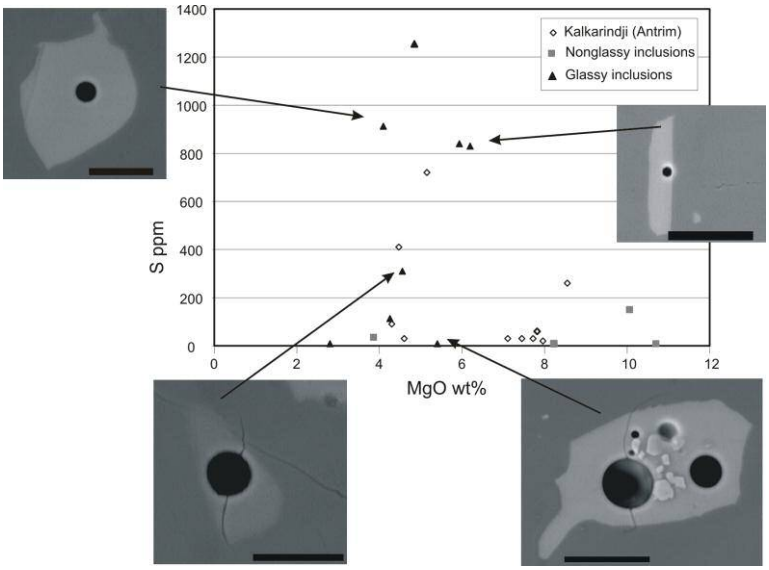

Fig. S9. *Sulfur content in glassy inclusions from EMP255, vs MgO wt%. Note that inclusions with low S content are associated with a crack through the inclusion and a large bubble, indicating loss of (volatile) material sometime during the heating-quenching treatment. The micrographs are BSE images: black scalebar is 20 µm. The amount of S those inclusions compare well with data from Kalkarindji (Antrim) lava flows (from (5)), suggesting these have been partially degassed.*

3.5. S and MgO of Whole-rock samples

Sulfur contents from 372 basalt samples range mostly from ca. 0 to 1900 µg/g, although a few rare analyses show content up to 7000 µg/g (Fig. S10A; Table S5). S is not correlated with MgO and the average S content (and standard deviation) is 884 ± 432 µg/g (Fig. 4).

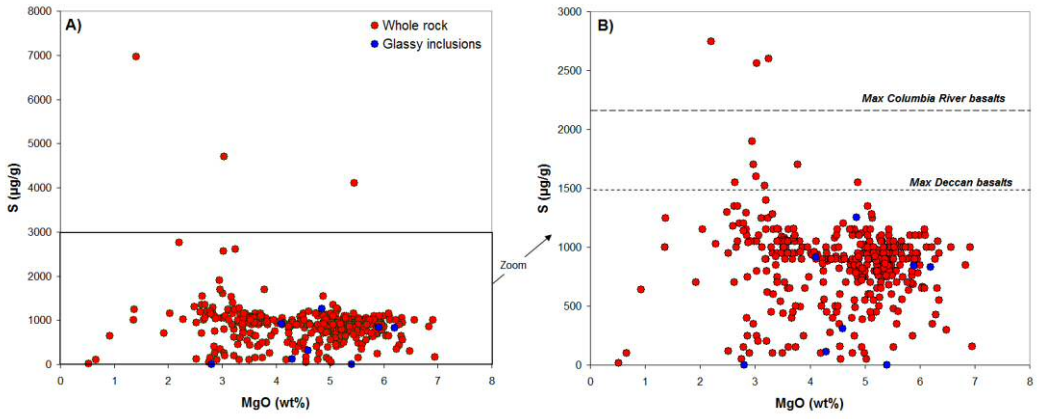

Fig. S10. *S (µg/g) vs. MgO (wt%) plot for Table Hill dolerites. A. whole data set. B. enlargement of A. Maximum values of Columbia River and Deccan basalts after Blake et al., (2010) and Black et al., 2012. Glassy inclusion analyses are shown for comparison and display a similar range of values compared to whole-rock analyses.*

3.6 Fractal analyses of the Blackfella Rockhole Member.

The Blackfella rockhole member is a ca. 70 m thick volcanic breccia unit that contains minor basaltic lavas (Fig. S11). It is spatially associated with the Bingy Bingy volcanic unit, a ca. 40 m thick glomeroporphyritic basalt that is slightly more evolved compared to the much thicker lava pile of the Antrim Plateau. The Bingy Bingy formation occurred over ca. 10,500 km² whereas the extent of the Blackfella formation is estimated to be at least 15,000 km².

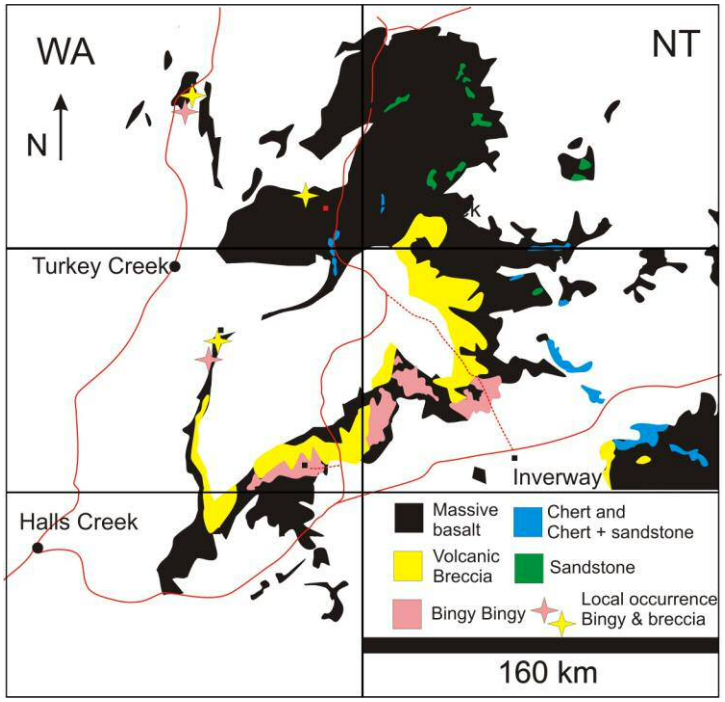

Fig. S11*: Field map showing the extent of the Blackfella Rockhole volcanic breccia (yellow), near the top of the Antrim Plateau Volcanics sequence (black).*

Fig. S12*: The Blackfella Rockhole volcanic breccia Member*

Fig. S132*: Volcanic bomb in the Blackfella Rockhole volcanic breccia Member*

Fractal analysis of breccia fragments from the Blackfella Rockhole member (Fig. S12, S13) was performed, to investigate the cause of fragmentation and the explosive potential of this

type of volcanism. We used (18) fractal spectrum technique for objectively classifying particles as (1) quench granulation, (2) magmatic blast/surge, (3) magmatic tephra fall and (4) phreatomagmatic. Shape files of 60 fragments from two samples (W03 and 099) from the Blackfella Rockhole Member have been analysed with this method (Fig. S14). The Fractal spectrum method indicates that, over 30 fragments, 11 clasts were fragmented by magmatic blast/surge, 14 by phreatomagmatic processes, and 5 by quench granulation for sample W03. for sample 099, similar results are observed with 17 clasts that were fragmented by magmatic blast/surge, 11 by phreatomagmatic processes, and 2 by quench granulation. In total, for the 60 fragments from the two samples, 47% of clasts were fragmented by magmatic blast/surge, 42% by phreatomagmatic processes, and 11% by quench granulation (Fig. S13). No tephra fall were apparent in our analyses. Therefore, these data suggest that the Blackfella Rockhole Member is the result of explosive fragmentation involving blast/surge and phreatomagmatic explosion due the interaction of magma with water.

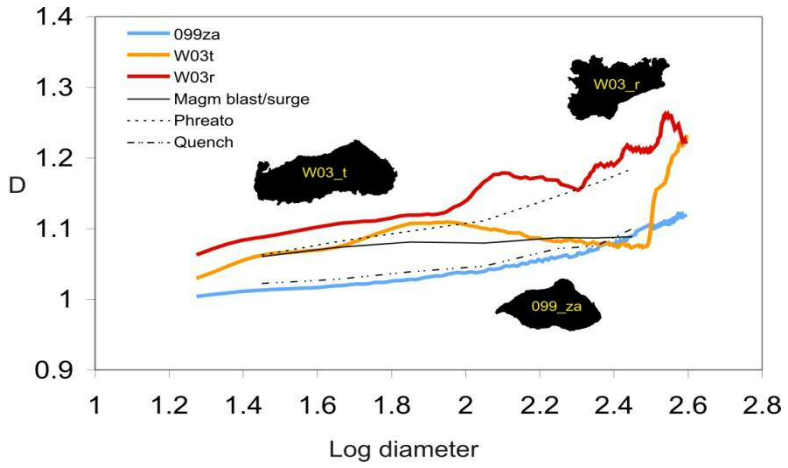

Fig. S14. *Examples of different types of volcanic breccias fragments identified by fractal analysis. Coloured curves and outlines are representative clasts of the three different fragmentation mechanisms identified; grey curves are from (18).*

4. Discussion

1. Sulfur degassed from the magma.

Both whole-rock and glassy inclusion S contents show a comparable range of values (Fig. 4 and S9). Fresh groundmass glass was absent from our sample suites preventing us to estimate the proportion of S that has been degassed from the magma. Nevertheless, we can compare our whole-rock data with similar data obtained from other LIPs, such as the Siberia or Deccan LIPs, within which basaltic flows have maximum S values of ~1700 and ~1400 µg/g and average values of ~800 and 850 µg/g, respectively (4, 17, 19). These studies showed that flows and intrusions have a degassing efficiency ranging between 50 and 90% (average ~64%). The range of values and average (~884 µg/g) of S contents obtained for the Table Hill Volcanics whole-rock samples compared to the maximum value of 1900 µg/g suggests that the that most of the magma has been fairly well degassed of its initial sulfur content. At face value, comparing the maximum value and the mean value, a crude estimation of 53% of S degassing can be calculated, in agreement with estimates calculated for other LIPs. The total S emission from the Kalkarindji province is hard to estimate because our knowledge of key parameters (i.e. the total volume of the province, the initial S content of the magma, the percentage of sulfate assimilation and the real degassing efficiency of each flow and sill) are ultimately not well constrained. Assuming a total area of the Kalkarindji LIP of 2.1×10^6 km², an average thickness of 1-1.5 km, an average rock density of 3.0 g/cm3, and a quantity of ~1215-1000 µg/g emitted (based on a maximum value of 1900 µg/g and a degassing percentage of 64-53%), the Kalkarindji LIP might have emitted between 6,350 and 11,500 Gt sulfur during its lifespan. Thermal plumes produced during eruptions (cf. discussion by (4) and references inside) and especially the occurrence of explosive breccias preserved in the

Kalkarindji volcanic stratigraphy (cf. above) suggest that a significant part of the S could have rise sufficiently high to reach the lower stratosphere. Finally, it should be stressed that these values do not account for the S that might have been directly degassed by contact metamorphism between intrusions and the abundant sulfate deposit of the Australian Central basins.

2. Randomness calculation

We have calculated the probability (P_{tot}) that large-scale continental volcanism and global extinction events are due to chance. Note that such calculations can be drastically improve and the following equations only provide a crude estimate. Nevertheless, this series of calculations suffice to demonstrate that the mass extinctions – LIP association cannot be due to chance with a probability of $6x10^{-9}$ % that the synchronicity between LIPs and mass extinctions is random.

The probability of $6x10^{-9}$ % is calculated by assuming that each province lasts 2 Ma (except Viluy traps, for which age uncertainties are considered to be 10 Ma), that each of the 7 mass extinctions lasts 1 Ma, and that the Phanerozoic extends from 550 Ma to the present day. The probability value calculated for each LIP is multiplied with the others.

$$Ptot = P_{(D)} * P_{(C)} * P_{(S)} * P_{(E)} * P_{(V)} * P_{(K)}$$

Where D=Deccan, C=CAMP, S=Siberia, E=Emeishan, V=Viluy and K=Kalkarindji

For a given flood basalt:

$$P(x) = [(N - n) * d_{(ME)}] / [d_{(Ph)} / d_{(LIP)}]$$

Where N is the total number of mass extinction; d(ME) is the duration of a mass extinction (ME) assumed to be 1 Ma, d(Ph) is the duration of the Phanerozoic which is 550 Ma and d(LIP) is the duration of the LIP volcanism arbitrarily set at 2 Ma (20) except for the Viluy trap where the uncertainty on the duration due to the preliminary measurement of (21) is conservatively set at 10 Ma.

n varies between 0 and 5 and depends on the number of P(x) already calculated. In other words, once the probability for a LIP to be associated with one of the 7 mass extinctions has been calculated, this mass extinction is removed from the total (i.e. starting with 7 mass extinctions, then 6, 5 … 1). For example, starting with the probability that the K/Pg boundary and the Deccan traps synchronicity is due to chance alone is 2.5% using n=0. Once the Deccan-K/Pg pair are removed from the total (n=1), the probability that the Tr/J boundary and CAMP synchronicity is due to chance alone is then 2.2%.

Caption extra tables

Table S5

S (µg/g) and MgO (wt%) content of gabbroic sills from the Table Hills volcanic, intersected by 15 bore holes drilled in the officer basins (Fig. 1). Analyses determined by ICP-EOSDrilling carried out by AusQuest Limited company. Coordinates for each bore hole and depth of each sample are provided. Start of each bore hole data are indicated in bold font.

Table S6

Table S6: Potential gas emissions for each individual short-lived single-pulse continental flood basalt provinces, depending on the nature of the country rocks intruded by the magma. Anne 10: Potential gas emissions for each individual short-lived single-pulse continental flood basalt province, depending on the nature of the country rocks intruded by the magma. Compiled after (4, 17, 19, 21 -26 and numerous references inside).

References for supporting material

1. Hanley LM, Wingate MTD (2000) A SHRIMP zircon age for an Early Cambrian dolerite dyke - an intrusive phase of the Antrim Plateau Volcanics of northern Australia. *Aust. J. Earth Sci.* **46**:1029-1040
2. Williams CT, Munro No. 1 well (W.A.) Canning Basin E.P. 3 well completion report. *West Australian Petroleum Pty. Limited*. 1972.
3. Grey K et al. (2005) Lithostratigraphic nomenclature of the Officer Basin and correlative parts of the Patterson Orogen, Western Australia. *Geological Survey of Western Australia Report* **93**.
4. Black BA, Elkins-Tanton, LT, Rowe MC, Peate IU (2012) Magnitude and consequences of volatile release from the Siberian Traps. *Earth Planet. Sci. Lett.* **317-318**:363-373.
5. Evins L, Jourdan F, Philips D (2009) The Cambrian Kalkarindji Large igneous province: extent and characteristics based on new $^{40}Ar/^{39}Ar$ and geochemical data. *Lithos* **110**:294-304.
6. Capill L, Jackson D. *Unpublished Ausquest Ltd report to WA Dept of Mines*, Perth, 72p.
7. Gerstenberger H, Haase G (1999) A highly effective emitter substance for mass spectrometric Pb isotope ratio determinations. *Chem. Geol.* **136**:309-312

8. Bowring JF, McLean NM, Bowring SA (2011) Engineering cyber infrastructure for U-Pb geochronology: Tripoli and U-Pb-Redux. *Geochem. Geophys. Geosyst.* **12**, Q0AA19.
9. Stacey JS, Kramers JD (1975) Approximation of terrestrial lead isotope evolution by a two-stage model. *Earth Planet. Sci. Lett.* **26**:207-221.
10. Jaffey AH, Flynn KF, Glendenin LE, Bentley WC, Essling AM (1971) Precision measurement of half-lives and specific activities of 235U and 238U: *Phys. Rev.* **C4**:1889-1906.
11. Ludwig KR (2003) User's manual for isoplot 3. 00: a geochronological toolkit for Microsoft Excel. Berkeley Geochronology Centre, Special Publication **4**, 1–77.
12. Jourdan F, Verati C, Féraud G (2006) Intercalibration of the Hb3gr 40Ar/39Ar dating standard. *Chem. Geol.* **231**:177–189.
13. Jourdan F, Renne PR (2007) Age calibration of the Fish Canyon sanidine 40Ar/ 39Ar dating standard using primary K-Ar standards. *Geochim. Cosmochim. Acta* **71**, 387-402.
14. Renne PR, Mundil R, Balco G, Min K, Ludwig KR (2010) Joint determination of 40K decay constants and 40Ar*/ 40K for the Fish Canyon sanidine standard, and improved accuracy for $^{40}Ar/^{39}Ar$ geochronology. *Geochim. Cosmochim. Acta* **74**: 5349-5367.
15. Koppers AAP (2002) ArArCALC-software for 40Ar/39Ar age calculations. *Comp. Geosci.* **28**:605–619.
16. A. Marzoli *et al.* (2011) Timing and duration of the Central Atlantic magmatic province in the Newark and Culpeper basins, eastern U.S.A. *Lithos* **122**:175-188.
17. Blake S, Self S, Sharma K, Sephton S (2010) Sulfur release from the Columbia River Basalts and other flood lava eruptions constrained by a model of sulfide saturation. *Earth Planet. Sci. Lett.* **299**: 328-338.

18. Maria A, Carey S (2007) Quantitative discrimination of magma fragmentation and pyroclastic transport processes using the fractal spectrum technique. *J. Volcanol. Geotherm. Res.* **161**:234-246.

19. Self S, Thordarson T, Widdowson M (2005) Gas Fluxes from Flood Basalt Eruptions. Elements **1**:283-287.

20. Courtillot VE, Renne PR (2003) On the ages of flood basalt events. *C. R. Geosci.* **335**: 113–140.

21. Courtillot V, Kravchinsky VA, Quidelleur X, Renne PR, Gladkochub DP (2010) Preliminary dating of the Viluy traps (Eastern Siberia): Eruption at the time of Late Devonian extinction events? *Earth Planet. Sci. Lett.* **300**: 239-245.

22. Shellnutt JG, Denyszyn SW, Mundil R (2010) Precise age determination of mafic and felsic intrusive rocks from the Permian Emeishan large igneous province (SW China). *Gond. Res.* **22**:118-126.

23. Schoene B, Guex J, Bartolini A., Schaltegger U, Blackburn TJ (2010) Correlating the end-Triassic mass extinction and flood basalt volcanism at the 100 ka level. *Geology* **38**:387-390.

24. Svensen H, Planke S, Polozov AG, Schmidbauer N, Corfu F, Podladchikov YY, Jamtveit B (2009) Siberian gas venting and the end-Permian environmental crisis. *Earth Planet. Sci. Lett.* **277**:490-500.

25. Ganino C, Arndt NT (2009) Climate changes caused by degassing of sediments during the emplacement of large igneous provinces. *Geology* **37**:323-326.

26. Jourdan F, Féraud G, Bertrand H, Watkeys MK, Renne PR (2008) $^{40}Ar/^{39}Ar$ ages of the sill complex of the Karoo large igneous province: implications for the Pliensbachian-Toarcian climate change. *Geochem. Geophys., Geosyst.* **9**:Q06009.

Table S5

Click here to download Supplemental file: Table S5 -WR Sulfur data.xls

Hole No	GDA E	GDA N	Sample No	From	To	Interval	MgO	S
	(m)	(m)		(m)	(m)	(m)	(wt%)	(µg/g)
07THD001	**340154**	**7367674**	**102813**	**61.9**	**62.1**	**0.2**	**3.49**	**1090**
07THD001			102814	66.0	66.2	0.2	0.92	638
07THD001			102815	69.9	70.1	0.2	3.23	619
07THD001			102816	70.9	71.1	0.2	1.40	6963
07THD001			102817	73.9	74.1	0.2	2.83	1294
07THD001			102818	77.9	78.1	0.2	3.18	1522
07THD001			102819	81.9	82.1	0.2	3.61	1150
07THD001			102820	85.9	86.1	0.2	3.54	1081
07THD001			102821	89.9	90.1	0.2	3.56	1060
07THD001			102822	93.9	94.1	0.2	3.47	537
07THD001			102823	97.9	98.1	0.2	3.55	1010
07THD001			102824	101.9	102.1	0.2	3.82	493
07THD001			102825	105.9	106.1	0.2	4.90	903
07THD001			102826	111.1	111.3	0.2	4.93	942
07THD001			102827	114.1	114.3	0.2	5.22	901
07THD001			102828	117.9	118.1	0.2	5.01	992
07THD001			102829	121.2	121.5	0.3	4.36	278
07THD001			102830	125.2	125.4	0.2	0.52	16
07THD001			102831	126.2	126.4	0.2	5.10	906
07THD001			102832	129.8	130.0	0.2	5.86	761
07THD001			102833	134.0	134.2	0.2	5.58	1015
07THD001			102834	138.1	138.3	0.2	5.53	475
07THD001			102835	142.2	142.4	0.2	2.28	1026
07THD001			102836	145.9	146.1	0.2	5.89	846
07THD001			102837	150.1	150.3	0.2	5.66	939
07THD001			102838	154.1	154.3	0.2	4.97	1020
07THD001			102839	158.1	158.3	0.2	5.26	1087
07THD001			102840	161.9	162.1	0.2	5.33	851
07THD001			102841	165.9	166.1	0.2	4.94	1119
07THD001			102842	169.9	170.1	0.2	4.53	819
07THD001			102843	174.2	174.4	0.2	4.48	921
07THD001			102844	177.9	178.1	0.2	5.88	246
07THD001			102845	180.1	180.3	0.2	4.55	160
07THD001			102846	181.0	181.2	0.2	4.45	1081
07THD002	**342847**	**7392547**	**103143**	**70.1**	**70.3**	**0.2**	**4.32**	**882**
07THD002			103144	74.1	74.3	0.2	4.02	952
07THD002			103145	78.1	78.3	0.2	4.04	931
07THD002			103146	82.1	82.3	0.2	4.26	556
07THD002			103147	86.1	86.3	0.2	4.74	856
07THD002			103148	90.1	90.3	0.2	4.58	896
07THD002			103149	94.1	94.3	0.2	4.76	887
07THD002			103150	98.1	98.3	0.2	4.87	744
07THD002			103151	102.1	102.3	0.2	5.26	571
07THD002			103152	106.1	106.3	0.2	5.28	764
07THD002			103153	110.1	110.3	0.2	5.60	455
07THD002			103154	114.1	114.3	0.2	4.96	390
07THD002			103155	118.1	118.3	0.2	5.06	602
07THD002			103156	122.1	122.3	0.2	5.88	687
07THD002			103157	126.1	126.3	0.2	6.29	429

07THD002			103158	130.1	130.3	0.2	6.05	662
07THD002			103159	134.1	134.3	0.2	5.68	558
07THD002			103160	138.3	138.5	0.2	5.85	695
07THD002			103161	142.1	142.3	0.2	5.80	636
07THD002			103162	146.1	146.3	0.2	5.96	779
07THD002			103163	150.1	150.3	0.2	5.79	907
07THD002			103164	154.1	154.3	0.2	5.56	955
07THD002			103165	158.1	158.3	0.2	5.95	940
07THD002			103166	162.1	162.3	0.2	5.23	980
07THD002			103167	166.1	166.3	0.2	4.62	925
07THD002			103168	170.1	170.3	0.2	4.50	1149
07THD002			103169	172.6	172.8	0.2	4.46	996
07THD002			103170	179.1	179.3	0.2	4.54	349
07THD002			103171	180.1	180.3	0.2	4.82	489
08THD004	**340653**	**7368377**	**104825**	**50.0**	**55.0**	**5.0**	**3.22**	**800**
08THD004			104826	55.0	60.0	5.0	3.32	950
08THD004			104827	60.0	65.0	5.0	3.63	950
08THD004			104828	65.0	70.0	5.0	4.26	900
08THD004			104829	70.0	75.0	5.0	4.94	800
08THD004			104830	75.0	80.0	5.0	5.11	700
08THD004			104831	80.0	85.0	5.0	5.01	750
08THD004			104832	85.0	90.0	5.0	5.36	750
08THD004			104833	90.0	92.9	2.9	5.21	450
08THD004			104834	100.0	100.2	0.2	5.87	950
08THD004			104835	105.1	105.3	0.2	5.19	900
08THD004			104836	110.1	110.3	0.2	5.29	700
08THD004			104837	115.1	115.3	0.2	5.21	800
08THD004			104838	120.1	120.3	0.2	4.84	800
08THD004			104839	123.0	123.2	0.2	4.21	500
08THD005	**340786**	**7369310**	**104899**	**35**	**40**	**5**	**3.03**	**800**
08THD005			104900	40	45	5	3.20	1400
08THD005			104901	45	50	5	3.85	900
08THD005			104902	50	55	5	4.41	900
08THD005			104903	55	60	5	4.73	800
08THD005			104904	60	65	5	4.81	1150
08THD005			104905	65	70	5	5.44	1100
08THD005			104906	70	75	5	5.45	1000
08THD005			104907	75	78	3	5.67	1050
08THD005			104908	78.1	78.3	0.2	6.91	1000
08THD005			104909	80.1	80.3	0.2	6.33	1050
08THD005			104910	85.1	85.3	0.2	4.78	1100
08THD005			104911	90.1	90.3	0.2	5.36	1000
08THD005			104912	95.1	95.3	0.2	5.34	800
08THD005			104913	100.1	100.3	0.2	5.26	500
08THD005			104914	105.3	105.5	0.2	3.66	400
08THD006	**339858**	**7367657**	**104992**	**49.0**	**54.0**	**5.0**	**3.32**	**100**
08THD006			104993	54.0	59.0	5.0	3.53	700
08THD006			104994	59.0	64.0	5.0	3.40	750
08THD006			104995	64.0	69.0	5.0	2.65	1000
08THD006			104996	70.4	70.6	0.2	2.64	1550
08THD006			104997	72.5	72.7	0.2	3.03	4700
08THD006			104998	77.4	77.6	0.2	3.25	2600

08THD006			104999	82.4	82.6	0.2	2.62	1350
08THD006			105000	86.8	87.0	0.2	1.36	1000
08THD006			104961	91.6	91.8	0.2	2.21	2750
08THD006			104962	96.7	96.9	0.2	3.02	1600
08THD006			104963	100.3	100.5	0.2	3.12	1250
08THD006			104964	104.7	104.9	0.2	2.97	1700
08THD006			104965	110.3	110.5	0.2	3.20	1150
08THD006			104966	115.5	115.7	0.2	3.78	1700
08THD006			104967	120.5	120.7	0.2	3.20	900
08THD006			104968	125.4	125.6	0.2	3.98	750
08THD006			104969	130.5	130.7	0.2	5.09	1050
08THD006			104970	135.5	135.7	0.2	5.34	900
08THD006			104971	140.3	140.5	0.2	5.01	1000
08THD006			104972	145.3	145.5	0.2	4.73	800
08THD006			104973	150.4	150.6	0.2	5.52	150
08THD006			104974	154.7	154.9	0.2	5.06	1000
08THD006			104975	160.1	160.3	0.2	5.99	1100
08THD006			104976	165.1	165.3	0.2	5.82	1100
08THD006			104977	170.1	170.3	0.2	4.89	1100
08THD006			104978	175.5	175.7	0.2	4.87	1550
08THD006			104979	180.4	180.6	0.2	5.06	1350
08THD006			104980	185.4	185.6	0.2	4.49	450
08THD006			103601	187.2	187.4	0.2	4.41	400
08THD007	**339863**	**7367666**	**103663**	**90.1**	**90.3**	**0.2**	**1.38**	**1250**
08THD007			103664	95.1	95.3	0.2	1.92	700
08THD007			103665	100.1	100.3	0.2	2.49	1300
08THD007			103666	105.1	105.3	0.2	2.98	1050
08THD007			103667	110.1	110.3	0.2	3.60	650
08THD007			103668	115.1	115.3	0.2	5.14	1250
08THD007			103669	120.1	120.3	0.2	2.95	1900
08THD007			103670	125.1	125.3	0.2	3.70	450
08THD007			103671	129.6	129.8	0.2	4.66	700
08THD007			103672	135.1	135.3	0.2	5.16	550
08THD007			103673	140.2	140.4	0.2	5.41	750
08THD007			103674	145.1	145.3	0.2	5.32	800
08THD007			103675	150.1	150.3	0.2	5.24	800
08THD007			103676	155.2	155.4	0.2	5.45	4100
08THD007			103677	160.1	160.3	0.2	5.45	1050
08THD007			103678	165.1	165.3	0.2	6.32	650
08THD007			103679	170.1	170.3	0.2	5.92	1100
08THD007			103680	175.2	175.4	0.2	5.67	1000
08THD007			103681	180.2	180.4	0.2	5.16	1000
08THD007			103682	185.3	185.5	0.2	5.11	600
08THD007			103683	189.6	189.8	0.2	4.81	550
08THD007			103684	190.3	190.5	0.2	6.48	300
08THD008	**340828**	**7367809**	**103753**	**48**	**52**	**4.0**	**2.79**	**150**
08THD008			103754	52	56	4.0	2.85	400
08THD008			103755	56	60	4.0	3.03	1050
08THD008			103765	60	65	5.0	2.84	1150
08THD008			103766	65	70	5.0	3.18	900
08THD008			103756	70.5	70.7	0.2	3.55	900
08THD008			103757	75.1	75.3	0.2	3.91	650

08THD008			103758	80.1	80.3	0.2	3.56	1000
08THD008			103759	85.1	85.3	0.2	4.28	900
08THD008			103760	90.1	90.3	0.2	5.11	900
08THD008			103761	95.1	95.3	0.2	5.31	850
08THD008			103762	100.1	100.3	0.2	5.39	800
08THD008			103763	105.1	105.3	0.2	2.52	950
08THD008			103764	110	110.2	0.2	2.62	700
08THD008			103767	115.2	115.4	0.2	5.55	800
08THD008			103768	120.1	120.3	0.2	6.83	850
08THD008			103769	125.1	125.3	0.2	5.95	950
08THD008			103770	130.1	130.3	0.2	6.35	950
08THD008			103771	135	135.2	0.2	6.00	850
08THD008			103772	140.1	140.3	0.2	6.28	900
08THD008			103773	145.1	145.3	0.2	6.57	1000
08THD008			103774	150.2	150.4	0.2	5.94	950
08THD008			103775	155	155.2	0.2	5.79	1000
08THD008			103776	160	160.2	0.2	5.70	1000
08THD008			103777	165.1	165.3	0.2	5.31	1050
08THD008			103778	170.2	170.4	0.2	5.02	1150
08THD008			103779	175.1	175.3	0.2	3.63	650
08THD008			103780	176.1	176.3	0.2	2.75	50
08THD009	**340176**	**7367683**	**103844**	**80.0**	**80.2**	**0.2**	**2.69**	**1350**
08THD009			103845	85.0	85.2	0.2	3.22	200
08THD009			103846	90.0	90.2	0.2	3.56	1050
08THD009			103847	95.1	95.3	0.2	3.73	1050
08THD009			103848	100.0	100.2	0.2	3.73	950
08THD009			103849	105.1	105.3	0.2	3.40	700
08THD009			103850	110.1	110.3	0.2	4.29	1000
08THD009			103851	115.1	115.3	0.2	5.12	950
08THD009			103852	120.1	120.3	0.2	5.17	800
08THD009			103853	125.1	125.3	0.2	5.44	950
08THD009			103854	130.1	130.3	0.2	5.49	850
08THD009			103855	135.1	135.3	0.2	5.34	850
08THD009			103856	140.2	140.4	0.2	5.75	900
08THD009			103857	145.1	145.3	0.2	5.95	900
08THD009			103858	150.1	150.3	0.2	6.10	1100
08THD009			103859	155.1	155.3	0.2	6.12	1000
08THD009			103860	160.1	160.3	0.2	5.32	1050
08THD009			103861	165.2	165.4	0.2	5.39	950
08THD009			103862	170.1	170.3	0.2	5.41	950
08THD009			103863	175.1	175.3	0.2	5.27	950
08THD009			103864	180.2	180.4	0.2	4.87	700
08THD009			103865	185.1	185.3	0.2	4.63	900
08THD010	**339948**	**7367407**	**104033**	**52**	**54**	**2**	**1.71**	
08THD010			104037	60.1	60.3	0.2	4.23	900
08THD010			104038	65.0	65.2	0.2	4.38	900
08THD010			104039	70.0	70.2	0.2	4.46	900
08THD010			104040	75.2	75.4	0.2	2.87	750
08THD010			104041	80.1	80.3	0.2	3.63	1050
08THD010			104042	85.1	85.3	0.2	3.71	1050
08THD010			104043	90.2	90.4	0.2	2.87	250
08THD010			104044	95.1	95.3	0.2	2.85	1100

08THD010			104045	100.1	100.3	0.2	3.42	1050
08THD010			104046	105.1	105.3	0.2	2.97	350
08THD010			104047	110.2	110.4	0.2	3.68	900
08THD010			104048	115.2	115.4	0.2	4.19	100
08THD010			104049	120.2	120.4	0.2	4.54	600
08THD010			104050	125.2	125.4	0.2	4.81	250
08THD010			104051	130.1	130.3	0.2	4.87	850
08THD010			104052	135.2	135.4	0.2	5.22	650
08THD010			104053	140.1	140.3	0.2	5.04	850
08THD010			104054	145.1	145.3	0.2	5.85	800
08THD010			104055	150.2	150.4	0.2	6.08	1150
08THD010			104056	155.2	155.4	0.2	5.52	1050
08THD010			104080	160.2	160.4	0.2	5.34	950
08THD010			104081	165.2	165.4	0.2	4.76	1150
08THD010			104086	190.1	190.3	0.2	4.11	1050
08THD010			104087	195.2	195.4	0.2	4.49	1100
08THD010			104088	200.1	200.3	0.2	4.61	1200
08THD011	**339805**	**7368492**	**104139**	**64**	**69**	**5**	**3.40**	**950**
08THD011			104140	69	74	5	3.61	1050
08THD011			104141	74	79	5	3.43	1150
08THD011			104142	79	84	5	4.31	950
08THD011			104143	84	88	4	3.07	1100
08THD011			104171	90.0	90.2	0.2	4.76	400
08THD011			104170	95.2	95.4	0.2	5.11	1150
08THD011			104169	100.1	100.3	0.2	5.44	1150
08THD011			104168	105.2	105.4	0.2	5.31	1050
08THD011			104167	110.1	110.3	0.2	5.82	1000
08THD011			104166	115.0	115.2	0.2	6.23	350
08THD011			104165	120.2	120.4	0.2	5.90	900
08THD011			104164	125.1	125.3	0.2	5.69	750
08THD011			104163	129.8	130.0	0.2	5.77	700
08THD011			104162	135.1	135.3	0.2	5.34	850
08THD011			104161	139.8	140.0	0.2	5.69	900
08THD011			104160	145.1	145.3	0.2	5.41	900
08THD011			104159	150.2	150.4	0.2	5.19	900
08THD011			104158	155.1	155.3	0.2	4.87	950
08THD011			104157	160.1	160.3	0.2	3.86	1000
08THD011			104156	165.2	165.4	0.2	3.96	1000
08THD011			104155	170.2	170.4	0.2	3.51	1000
08THD011			104154	175.1	175.3	0.2	3.48	950
08THD011			104153	180.2	180.4	0.2	3.33	1150
08THD011			104152	184.8	185.0	0.2	3.23	1250
08THD011			104151	190.0	190.2	0.2	3.50	100
08THD011			104150	195.2	195.4	0.2	2.04	1150
08THD011			104149	199.8	200.0	0.2	3.45	1050
08THD011			104148	205.1	205.3	0.2	3.81	1050
08THD011			104147	209.8	210.0	0.2	3.60	1050
08THD012	**339954**	**7367417**	**104213**	**60.2**	**60.4**	**0.2**	**3.68**	**950**
08THD012			104214	65.1	65.3	0.2	4.53	1000
08THD012			104215	70.2	70.4	0.2	4.24	800
08THD012			104216	75.2	75.4	0.2	4.24	700
08THD012			104217	80.2	80.4	0.2	3.73	1100

08THD012			104218	85.1	85.3	0.2	3.56	1050
08THD012			104219	90.2	90.4	0.2	2.72	1200
08THD012			104220	95.2	95.4	0.2	2.69	1050
08THD012			104221	100.2	100.4	0.2	3.33	600
08THD012			104222	105.2	105.4	0.2	2.92	1050
08THD012			104223	110.2	110.4	0.2	3.55	1050
08THD012			104224	115.1	115.3	0.2	3.03	250
08THD012			104225	120.2	120.4	0.2	3.71	1050
08THD012			104226	125.1	125.3	0.2	4.10	950
08THD012			104227	130.1	130.3	0.2	3.88	250
08THD012			104228	135.1	135.3	0.2	4.81	850
08THD012			104229	140.1	140.3	0.2	5.12	400
08THD012			104230	145.0	145.2	0.2	5.57	800
08THD012			104231	150.4	150.6	0.2	3.61	150
08THD012			104232	155.1	155.3	0.2	5.11	450
08THD012			104233	160.1	160.3	0.2	2.90	100
08THD012			104234	165.1	165.3	0.2	6.04	650
08THD012			104235	170.1	170.3	0.2	6.35	550
08THD012			104236	175.1	175.3	0.2	6.08	650
08THD012			104237	180.4	180.6	0.2	5.64	850
08THD012			104238	185.2	185.4	0.2	4.46	500
08THD012			104239	190.2	190.4	0.2	5.74	1000
08THD012			104240	195.0	195.2	0.2	5.31	1100
08THD012			104241	200.1	200.3	0.2	4.94	150
08THD012			104242	202.1	202.3	0.2	3.75	150
08THD013	**339958**	**7367401**	**104287**	**70.1**	**70.3**	**0.2**	**4.11**	**900**
08THD013			104288	75.3	75.5	0.2	3.30	450
08THD013			104289	80.1	80.3	0.2	3.75	500
08THD013			104290	85.1	85.3	0.2	3.60	1050
08THD013			104291	90.3	90.5	0.2	3.30	1000
08THD013			104292	95.3	95.5	0.2	2.79	1200
08THD013			104293	100.8	101	0.2	4.78	100
08THD013			104294	105.1	105.3	0.2	3.05	200
08THD013			104295	110.2	110.4	0.2	3.40	1050
08THD013			104296	115	115.2	0.2	3.60	950
08THD013			104297	120.1	120.3	0.2	3.38	850
08THD013			104298	125.3	125.5	0.2	4.51	500
08THD013			104299	130.1	130.3	0.2	5.01	550
08THD013			104300	135.1	135.3	0.2	4.99	100
08THD013			104301	140.1	140.3	0.2	5.74	1000
08THD013			104302	145.2	145.4	0.2	5.21	800
08THD013			104303	150.2	150.4	0.2	4.89	850
08THD013			104304	155.1	155.3	0.2	5.37	900
08THD013			104305	160	160.2	0.2	5.16	950
08THD013			104306	165.1	165.3	0.2	5.27	900
08THD013			104307	168.6	168.8	0.2	5.34	1000
08THD013			104308	174.2	174.4	0.2	5.69	900
08THD013			104309	180.1	180.3	0.2	5.54	1000
08THD013			104310	185	185.2	0.2	5.21	950
08THD013			104311	190	190.2	0.2	5.37	850
08THD013			104312	195.1	195.3	0.2	5.29	1050
08THD013			104313	200.1	200.3	0.2	5.06	1100

08THD013			104314	205.2	205.4	0.2	5.29	650
08THD013			104315	209.3	209.5	0.2	4.73	1150
08THD014	**340652**	**7368357**	**104374**	**65.2**	**65.4**	**0.2**	**4.56**	**50**
08THD014			104375	70	70.2	0.2	5.02	50
08THD014			104376	74.8	75	0.2	5.01	800
08THD014			104377	80	80.2	0.2	5.21	800
08THD014			104378	85.5	85.7	0.2	5.22	850
08THD014			104379	90.3	90.5	0.2	5.52	900
08THD014			104380	95.2	95.4	0.2	5.59	350
08THD014			104381	100	100.2	0.2	6.22	1000
08THD014			104382	105.1	105.3	0.2	5.16	950
08THD014			104383	110.2	110.4	0.2	5.49	600
08THD014			104384	115.1	115.3	0.2	5.59	700
08THD014			104385	120.1	120.3	0.2	4.31	450
THC001	**417411**	**7321425**	**373545**	**0**	**3**	**3**	**0.66**	**100**
THC001			373546	3	5	2	2.52	120
THC001			373547	5	10	5	3.51	440
THC001			373548	10	15	5	5.12	1280
THC001			373549	15	20	5	4.14	940
THC001			373550	20	25	5	3.83	960
THC001			373551	25	30	5	3.13	1000
THC001			373552	30	35	5	2.6	1180
THC001			373553	35	40	5	2.79	1140
THC001			373554	40	45	5	3.32	1280
THC001			373555	45	50	5	3.4	1160
THC001			373556	50	55	5	3.71	1160
THC001			373557	55	60	5	3.7	1080
THC001			373558	60	65	5	3.73	1100
THC001			373559	65	70	5	4.1	940
THC001			373560	70	75	5	4.24	860
THC001			373561	75	80	5	4.78	900
THC001			373562	80	85	5	4.84	900
THC001			373563	85	90	5	4.96	820
THC001			373564	90	95	5	5.21	880
THC001			373565	95	100	5	5.45	840
THC001			373566	100	105	5	5.37	780
THC001			373567	105	110	5	5.45	800
THC001			373568	110	115	5	5.5	760
THC001			373569	115	120	5	5.42	840
THC001			373570	120	125	5	5.36	900
THC001			373571	125	130	5	5.04	940
THC001			373572	130	135	5	4.92	1020
THC001			373573	135	140	5	4.89	920
THC001			373574	140	145	5	4.97	740
THC001			373575	145	150	5	6.95	160
THC002	**417207**	**7321426**	**373596**	**5**	**15**	**10**	**2.88**	**1040**
THC002			373597	15	25	10	3.38	920
THC002			373598	25	30	5	3.53	1000
THC002			373599	30	35	5	4.08	960
THC002			373600	35	40	5	4.39	900
THC002			373601	40	45	5	4.84	780
THC002			373602	45	50	5	5.24	760

THC002	373603	50	55	5	5.34	820
THC002	373604	55	60	5	5.39	760
THC002	373605	60	65	5	5.24	800
THC002	373606	65	70	5	5.44	680
THC002	373607	70	75	5	5.22	800
THC002	373608	75	80	5	5.19	920
THC002	373609	80	85	5	4.96	740
THC002	373610	85	90	5	4.94	720
THC002	373611	90	95	5	5.36	860
THC002	373612	95	100	5	5.06	900
THC002	373613	100	105	5	3.03	2560

Table 1: S (µg/g) and MgO (wt%) content of gabbroic sills from the Table Hills volcanic, intersected by 15 bore holes drilled in the officer basins (Fig. 1). Analyses determined by ICP-EOSDrilling carried out by AusQuest Limited company. Coordinates for each bore holes and depth of each samples are provided. Start of each bore hole data indicated in bold font.

Table S6

Click here to download Supplemental file: Table S6 - Relationship gases + provinces.xls

Province	Age (Ma)	Size (km²)	Significant extinction	Major AOE	$\delta^{13}C$	Eruption rate (duration peak; Ma)	Mantle CO_2 and SO_2	Evaporites (SO_2; Halocarbon)	Oil /gas ± Shale (CH_4)	Coal (CO_2)	Dolostone (CO_2)
Deccan	66	$1x10^6$	Cretaceous / Paleogene	No	Yes	Fast (<2Ma)	Likely	No	**Yes**	No	No
Parana-Etendeka	132	$2x10^6$	No	No	No	Fast to Moderate (2-3Ma)	Likely	Yes	No	**Yes**	No
Karoo	182	$3x10^6$	No	Yes	Yes	Slow (~3-4 Ma)	Likely	No	No	**Yes**	No
CAMP	201	$10x10^6$	Triassic/Jurassic	No	Yes	Fast (<2Ma)	Likely	**Yes**	**Yes**	No	**Yes**
Siberia	252	$4x10^6$	Permian/Triassic	No	Yes	Fast (<2Ma)	Likely	**Yes**	**Yes**	**Yes**	**Yes**
Eimeshan	259	$>0.5x10^6$	End Guadalupian	No	Yes	Fast (<2Ma)	Likely	No	**Yes**	No	**Yes**
Viluy	274	?	Frasnian-Fammenian	No	Yes	Unknown	Likely	Unknown	Unknown	Unknown	**Yes**
Kalkarindji	510	$2x10^6$	Early-Middle Cambrian	No	Yes	Fast? (<<3 Ma)	Likely	**Yes**	**Yes**	No	**Yes**

Table S6: Jourdan et al.